

## Reversing Signs of Parkinsonism in a Cell Model Using Mitochondria-Targeted Organoiridium Catalysis

Rahul D. Jana, Hieu D. Nguyen, Guangjie Yan, Tai-Yen Chen, and Loi H. Do\*

Cite This: <https://doi.org/10.1021/acs.jmedchem.4c02741>

Read Online

ACCESS |



Metrics &amp; More

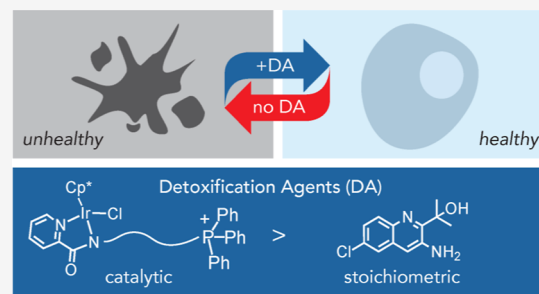


Article Recommendations



Supporting Information

**ABSTRACT:** We report the application of organoiridium complexes as catalytic agents for the detoxification of biogenic reactive aldehyde species (RASP), which are implicated in the pathogenesis of neurodegenerative disorders. We show that Ir complexes functionalized with phosphonium cations localize selectively in the mitochondria and have better cellular retention compared to that of their parent Ir species. In a cell model for Parkinsonism, the mitochondria-targeted iridium catalysts exhibited superior cell protecting abilities and longer-lasting effects (up to 6 d) than conventional RASP scavengers, which failed to be effective beyond 24 h. Our biological assays indicate that treatment with the Ir compounds led to reduction in reactive oxygen species and aldehyde levels while partially preserving the native mitochondrial membrane potential and NAD<sup>+</sup>/NADH ratio in 1-methyl-4-pyridinium-inhibited cells. Our work is the first to demonstrate catalytic nonenzymatic detoxification of RASP in living systems.



## INTRODUCTION

Parkinson's disease (PD) is the second most prevalent neurodegenerative disorders globally, affecting up to 1–4% of the population over 65 years old.<sup>1–5</sup> The clinical presentation of PD often includes impaired motor (e.g., bradykinesia, rigidity, etc.) and nonmotor (e.g., depression, anxiety, etc.) functions (Chart 1A). On the cellular level, PD is characterized by abnormalities in the mitochondria, lysosome, and endosome and gradual loss of dopaminergic neurons.<sup>5,6</sup> Although the exact cause of PD is still unknown, its pathogenesis has been linked to  $\alpha$ -synuclein aggregation into Lewy bodies and neurites that lead to toxic gain of function.<sup>7–10</sup> There are currently no cures for PD but treatments can help with managing symptoms (Chart 1B).<sup>11–13</sup> For example, the dopamine precursor levodopa (L-Dopa) is used to alleviate many of the motor issues of PD in its early stages. It is often prescribed in conjunction with carbidopa (CD), a decarboxylase inhibitor that reduces extracerebral metabolism of L-Dopa so that it can persist in the body long enough to cross the blood–brain barrier (BBB). However, long-term use of L-Dopa can cause significant side effects,<sup>14–16</sup> including drug-induced dyskinesia. Other PD treatments that focus on controlling neurotransmitter levels include dopamine agonists, monoamine oxidase B inhibitors, N-methyl-D-aspartate glutamate receptor antagonists, and others.

Mitochondrial dysfunction and oxidative stress are now widely recognized as key contributors to PD.<sup>17,18</sup> There is increasing evidence showing that deficiency in the respiratory Complex I (C-I)<sup>19,20</sup> within the mitochondria of dopaminergic neurons results in redox imbalance and elevated reactive

oxygen species (ROS) production.<sup>21,22</sup> Such ROS-induced oxidative stress contributes to neuronal degeneration by damaging lipids, proteins, and nucleic acids. A wide range of mitochondria-targeted organic compounds have been studied in PD research.<sup>23–25</sup> Among these, the antioxidant Coenzyme Q10 (CoQ10) has undergone phase 3 clinical trials with mixed results.<sup>26–28</sup> Although CoQ10 was well tolerated in people, it did not improve the motor symptoms of PD.<sup>26,29</sup> Another antioxidant that can penetrate the BBB is MitoQ, which is composed of ubiquinone conjugated to a triphenylphosphonium moiety and is available commercially as a supplement to enhance mitochondrial function and energy. Unfortunately, it has failed to show efficacy in clinical trials.<sup>30</sup>

In search for more effective PD treatments, researchers have focused on reactive aldehyde species (RASP) as possible therapeutic targets.<sup>31–38</sup> RASP, which include formaldehyde, 4-hydroxynon-2-enal (4-HNE or Ia), acrolein, malondialdehyde, and crotonaldehyde, can be acquired from the environment, food/drink, and biological degradation of lipids and carbohydrates. The accumulation of neurotoxic aldehydes, such as 2,3-dihydroxyphenylacetaldehyde (DOPAL or IIa), is due to altered monoamine metabolism.<sup>37,39–41</sup> Because RASP are potent electrophiles, they react readily with nucleophilic

Received: November 9, 2024

Revised: December 6, 2024

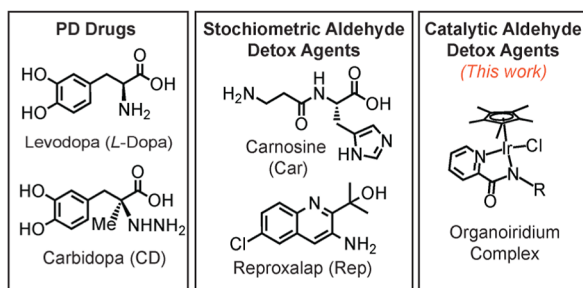
Accepted: December 26, 2024

**Chart 1. (A) Typical Hallmarks of Parkinson's Disease and (B) Small Molecule Therapeutics Currently Used or under Investigation for Its Treatment**

A) Hallmarks of Parkinson's Disease

	<b>Clinical</b> <ul style="list-style-type: none"> <li>• Impaired motor functions (e.g., bradykinesia, rigidity, etc.)</li> <li>• Impaired non-motor functions (e.g., depression, anxiety, etc.)</li> </ul>
	<b>Cellular</b> <ul style="list-style-type: none"> <li>• Abnormal mitochondria, lysosome, and endosome functions</li> <li>• Loss of dopaminergic neurons</li> </ul>
	<b>Molecular</b> <ul style="list-style-type: none"> <li>• <math>\alpha</math>-Synuclein aggregation (e.g., Lewy bodies and neurites)</li> <li>• Elevated reactive oxygen species</li> <li>• Lipid peroxidation and aldehyde accumulation</li> </ul>

B) Small-Molecule Therapeutics



groups in biomolecules and can induce protein aggregation via covalent cross-linking.<sup>35</sup> RASP have been implicated in the formation of  $\alpha$ -synuclein oligomers that can damage lipid membranes and be transmitted from unhealthy to healthy neurons, which may lead to exacerbation of PD.<sup>10,35,41–43</sup> Although there are natural defense systems against RASP,<sup>44</sup> they are often deficient in sick patients.

As an intervention, the use of RASP detoxification (detox) agents that assist in their biological clearance has shown promise in some studies.<sup>45–49</sup> These compounds typically feature primary amine or hydrazine groups that react with aldehydes to form nontoxic imine or hydrazone species, respectively. A variety of drugs and natural compounds exhibit aldehyde scavenging properties, including metformin, aminoguanidine, pyridoxamine, thiamine, and carnosine (Car) (Chart 1B). The drug candidate reproxalap (Rep) is currently in phase 3 clinical trials as a RASP scavenger to treat eye inflammation.<sup>50,51</sup> All of these compounds are stoichiometric reactants, which means that each RASP detox agent can react with only a single aldehyde molecule. Because of their stoichiometric nature, RASP scavengers likely need to be administered on a frequent basis to achieve their therapeutic effects.

Based on the current understanding of PD etiology, we hypothesized that catalytic aldehyde detoxification in the mitochondria could offer selective defense against toxicants that contribute to PD pathogenesis. We showed in previous work that untargeted  $[\text{Cp}^*\text{Ir}(\text{picolinamidate})\text{Cl}]$  complexes ( $\text{Cp}^*$  = pentamethylcyclopentadienyl anion, Chart 1B) are capable of protecting mammalian cells from RASP damage by converting them to unreactive alcohols via a transfer hydrogenation mechanism.<sup>52,53</sup> In the present study, we designed Ir complexes that are capable of selectively accumulating in the mitochondria and leveraged their reductase-like properties to enhance mitochondrial integrity and cell growth in cellular models of PD. We show that

mitochondria-targeted Ir catalysts exhibit greater biological activity compared to that of their nontargeted counterparts and demonstrate that catalytic Ir detox agents display longer-lasting effects than conventional RASP scavengers over a multiple-days time course. Most notably, the Ir detox agents reversed key cellular biomarkers associated with Parkinsonism, suggesting that they may be candidates for further development as therapeutics.

## RESULTS AND DISCUSSION

**Catalyst Design, Synthesis, and Characterization.** In previous studies, we demonstrated that  $[\text{Cp}^*\text{Ir}(\text{picolinamidate})\text{Cl}]$  complexes are competent catalysts for aldehyde reduction in the presence of a hydride source (e.g., sodium formate or reduced nicotinamide adenine dinucleotide, NADH) under biologically relevant conditions<sup>54</sup> and inside living environments.<sup>52,53</sup> Because mitochondria dysfunction is a common hallmark of PD,<sup>6,20,55</sup> we proposed that targeting our Ir catalysts to this organelle could amplify their therapeutic effects since it could potentially intercept RASP at the site of generation (e.g., due to lipid peroxidation of the mitochondrial membrane).<sup>21</sup> The parent catalyst **Ir1**, which bears an *N*-phenylpicolinamidate ligand, was prepared based on a literature procedure.<sup>56</sup> To create the mitochondria-targeted catalysts,<sup>24,57</sup> we attached phosphonium groups to our Ir complex to form two different variants, the non-emissive **Ir2<sub>mito</sub>** and the emissive **Ir3<sub>mito</sub>** due to the presence of a pyrene moiety (Figure 1A).<sup>58</sup> For comparison, we also prepared the nontargeted derivatives **Ir2** and **Ir3**, which lack the phosphonium groups of **Ir2<sub>mito</sub>** and **Ir3<sub>mito</sub>**, respectively. Due to the poor water solubility of **Ir3**, we also prepared **Ir3'** that contains a pyrene unit attached to the picolinamidate ligand via a short amide linker.

To obtain the new picolinamide ligands, two different routes were pursued. The first route involves amide coupling between picolinic acid and a primary amine to furnish the corresponding **L2** ( $R = \text{decyl}$ ), **L2<sub>mito</sub>** ( $R = \text{decyl-triphenylphosphonium bromide}$ ), **L3** ( $R = \text{undecyl-pyrene}$ ), and **L3'** ( $R = \text{carbamoyl-pyrene}$ ) ligands with up to  $\sim 70\%$  yield (Figure 1B). The second route involves preparing the picolinamide **7** from picolinic acid and *N*-(10-bromodecyl)-amine, followed by nucleophilic substitution with diphenylpyrenylphosphine to provide **L3<sub>mito</sub>** in 32% yield (Figure 1C). Metalation of the final picolinamide ligands with  $[\text{Cp}^*\text{IrCl}_2]_2$  in the presence of triethylamine gave the Ir complexes **Ir2**, **Ir2<sub>mito</sub>**, **Ir3**, **Ir3'**, and **Ir3<sub>mito</sub>** in moderate to good yields ( $\sim 70\text{--}80\%$ ) after purification. The complexes were fully characterized by a variety of spectroscopic techniques (NMR, IR, and UV–vis absorption) and mass spectrometry.

The emissive compounds were further characterized by fluorescence spectroscopy (Figure 1D). In dichloromethane, excitation of **Ir3**, **Ir3'**, and **Ir3<sub>mito</sub>** (30  $\mu\text{M}$ ) at 340 or 350 nm produced emission spectra showing vibrational fine structure between 360 and 520 nm that is characteristic of the pyrene unit.<sup>59</sup> Because **Ir3<sub>mito</sub>** was soluble in phosphate buffered saline (PBS), its fluorescence spectrum was also measured in this solvent, showing peaks at  $\sim 390$  and 400 nm that are similar to those observed in  $\text{CH}_2\text{Cl}_2$  but with lower intensity. To obtain the fluorescence spectrum of **Ir3'** in aqueous solution, a mixture of PBS/DMSO (95:5) was used (Figure 1D, middle). The emission spectrum clearly showed the presence of the pyrene moiety with fluorescence bands at  $\sim 390$  and 400 nm.

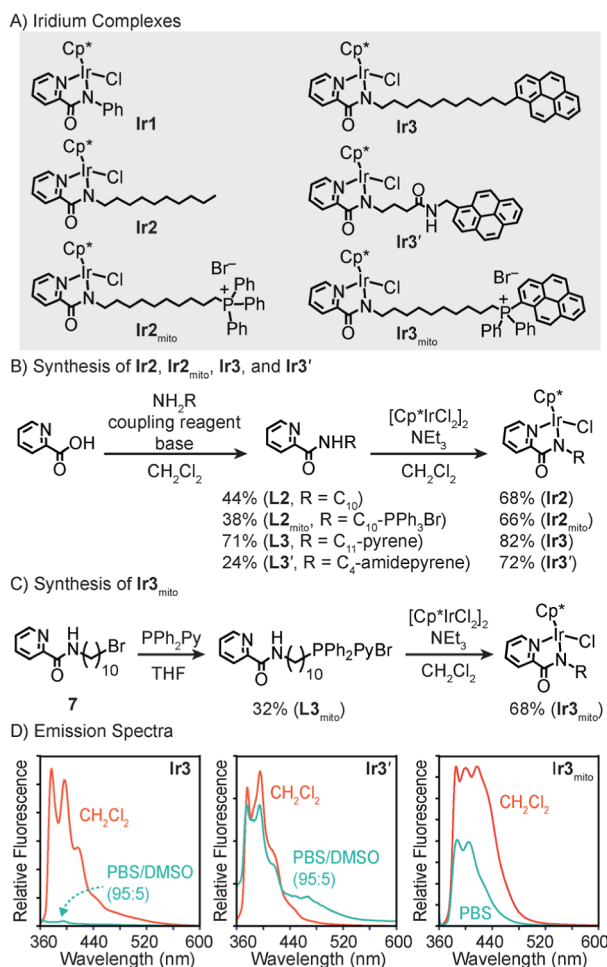


**Figure 1.** (A) Structures of the iridium complexes used in this study; (B,C) synthesis of the iridium complexes; and (D) emission spectra of Ir3, Ir3', and Ir3<sub>mito</sub> (30  $\mu$ M,  $\lambda_{ex}$  = 340 or 350 nm). Abbreviations: Cp\* = pentamethylcyclopentadienyl anion, Py = pyrene.

Unfortunately, the poor solubility of Ir3 in PBS/DMSO (95:5) precluded its measurement in aqueous solution.

**Transfer Hydrogenation Studies.** To evaluate the reductase-like activity of the Ir complexes,<sup>60</sup> we subjected them to transfer hydrogenation studies using biogenic aldehydes that have been linked to PD pathogenesis.<sup>38</sup> The first substrate we tested was Ia,<sup>32,35,36,61</sup> which is a toxic byproduct of lipid peroxidation that has been shown to alkylate biomolecules and cause protein aggregation. When Ia was combined with an Ir complex (1 mol % relative to the substrate) and excess HCOONa in PBS/DMSO (95:5) at 37 °C for 24 h, the products 4-hydroxynon-2-en-1-ol (Ib) and 4-hydroxynon-1-ol (Ic) were obtained in all cases (Figure 2A). Because reduction likely proceeds from Ia  $\rightarrow$  Ib  $\rightarrow$  Ic,<sup>52</sup> the amount of Ic obtained is an indicator of the catalyst's relative reactivity. Our results suggest that the mitochondria-targeted catalysts are more active than their nontargeted variants (e.g., Ir2<sub>mito</sub> > Ir2 and Ir3<sub>mito</sub> > Ir3'). Complex Ir3 was not tested due to its poor aqueous solubility. Relative to the parent catalyst Ir1, which gave 86% yield of Ic, Ir2<sub>mito</sub> was equally active (85%) and Ir3<sub>mito</sub> was less active (21%). Based on our previous studies, functionalization at the N-phenyl moiety of the picolinamidate ligand should have minimum effects on the iridium reactivity.<sup>60</sup> However, the lower yield of Ir2, and Ir3<sub>mito</sub> compared to that of Ir1 is likely due to their reduced

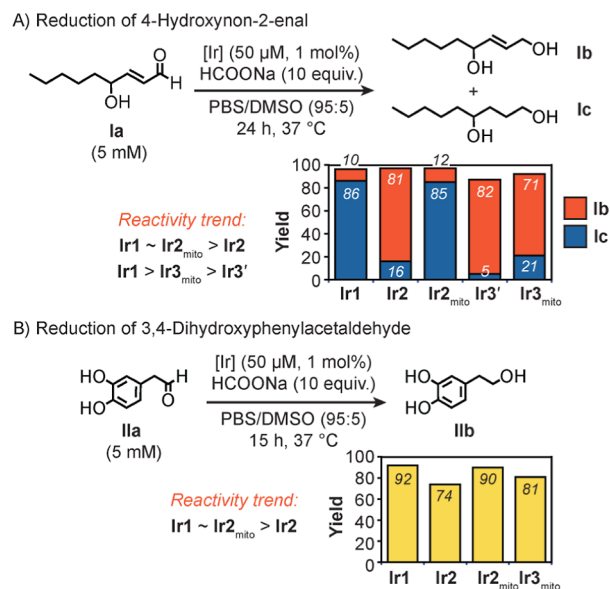


**Figure 2.** Transfer hydrogenation studies using 4-hydroxynon-2-enal (A) and 3,4-dihydroxyphenylacetaldehyde (B) as substrates with the iridium catalysts.

solubility in the PBS/DMSO reaction mixture. In fact, we observed small but visually detectable amounts of yellow Ir2 precipitate in the reaction over the course of several hours. Because Ir3' has an additional pendant amide group, it can potentially bind and coordinatively inhibit the iridium center. Despite their differences in activity, all the Ir complexes tested were active for transfer hydrogenation under biologically relevant conditions.

The second biogenic substrate we used was IIa, which is derived from cellular metabolism of the neurotransmitter dopamine and is believed to trigger  $\alpha$ -synuclein oligomerization that can impair synaptic functions.<sup>37,39–41</sup> In these experiments, the same reaction conditions were employed as described above by combining IIa with an Ir catalyst and HCOONa in PBS/DMSO (95:5) (Figure 2B). After 15 h, Ir1, Ir2, Ir2<sub>mito</sub>, and Ir3<sub>mito</sub> afforded 2-(3,4-dihydroxyphenyl)ethanol (IIb) in 92, 74, 90, and 81% yields, respectively. Once again, Ir2<sub>mito</sub> exhibited similar activity as that of Ir1 but Ir2 and Ir3<sub>mito</sub> were slightly lower. These solution studies suggest that our Ir complexes are promising candidates for therapeutic applications due to their ability to transform RASP into unreactive products.

**Biological Properties of the Ir Complexes.** Before conducting the PD cell model studies, we investigated the biological properties of our Ir complexes. We have shown in previous work that [Cp\*Ir(picolinamidate)Cl] species are chemically stable in aqueous solutions and biological media for at least several days or longer.<sup>60</sup> To assess the aqueous stability of the mitochondria-targeted catalysts, we measured their NMR spectra in D<sub>2</sub>O/DMSO-*d*<sub>6</sub> (90:10). Our data showed that the <sup>1</sup>H NMR spectra of Ir2<sub>mito</sub> (Figure S3) and Ir3<sub>mito</sub> (Figure S6) were unchanged over the course of 48 h, indicating that no degradation had occurred.

Next, we determined the octanol/PBS partition coefficients (Log *P*) of the Ir complexes,<sup>62</sup> which provide an estimate of the compounds' lipophilicity (i.e., >0 = more lipophilic and <0 = more hydrophilic). The Ir compounds were dissolved in an octanol/PBS mixture with different ratios and then the amount

distributed in each phase was measured by UV–vis absorption spectroscopy. Our data revealed the following Log *P* trend: **Ir3** ( $1.86 \pm 0.19$ ) > **Ir2** ( $1.47 \pm 0.20$ ) > **Ir3<sub>mito</sub>** ( $1.21 \pm 0.09$ ) > **Ir1** ( $1.15 \pm 0.23$ ) > **Ir3'** ( $1.13 \pm 0.10$ ) > **Ir2<sub>mito</sub>** ( $0.94 \pm 0.12$ ) (Figure S14). These results corroborate the poor water solubility of **Ir3** and the lipophilicity tracks somewhat with catalyst activity (Figure 2), in which more water-soluble catalysts (e.g., **Ir2<sub>mito</sub>**) tend to display higher transfer hydrogenation rates than their less water-soluble counterparts (e.g., **Ir2**).

To study cell uptake, we used inductively coupled plasma mass spectrometry (ICP–MS) to quantify the amount of iridium inside cells after treatment with the catalysts for various lengths of time. We performed studies in human neuroblastoma SH-SY5Y cells because they are commonly used as *in vitro* models for PD research.<sup>63–65</sup> After exposing the cells to 5  $\mu\text{M}$  of the Ir complexes for 3 h, analysis of the resulting cell lysates showed that iridium was present in all samples, ranging from 34 to 213 ng/10<sup>6</sup> cells (Table S1). The Ir cell accumulation was observed in the following order: **Ir2** > **Ir1** > **Ir3'** > **Ir2<sub>mito</sub>** > **Ir3<sub>mito</sub>** > **Ir3**. A plot of the Log *P* vs Ir uptake concentration does not show a strong correlation between these two parameters (Figure 3A, left). Because our Ir catalysts have different overall charges, shapes, and sizes, these factors could potentially impact their mode and efficiency of cellular uptake.

To investigate the cell retention of our Ir complexes, we measured the iridium content in cells after incubation post-treatment in fresh cell culture media for various amounts of time (Table S2). As shown in Figure 3A (right), the intracellular Ir concentrations decreased after 24 and 48 h.

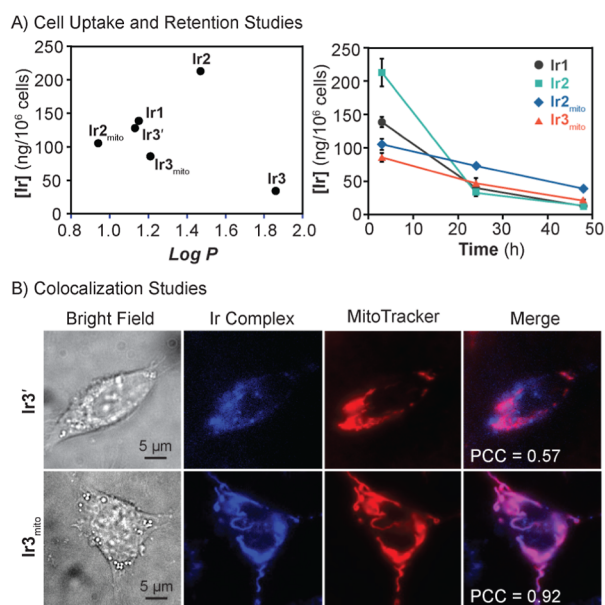


**Figure 3.** (A) Cellular uptake of the iridium complexes as a function of their Log *P* values (left, 3 h incubation) and their cellular retention over time (right). The SH-SY5Y cells were treated with 5  $\mu\text{M}$  of the Ir complexes and the Ir concentrations were quantified using ICP–MS. Log *P* was measured using the shake-flask method. (B) Microscopy images of SH-SY5Y cells treated with either **Ir3'** or **Ir3<sub>mito</sub>** (5  $\mu\text{M}$ ) for 2 h and then MitoTracker Deep Red (10 nM) for 20 min. The Ir complexes were excited at 405 nm and emission was recorded using a 438/24 nm filter, whereas MitoTracker Deep Red was excited at 640 nm and emission was recorded using a 680/42 nm filter.

The mitochondria-targeted catalysts **Ir2<sub>mito</sub>** and **Ir3<sub>mito</sub>** were retained better than the nontargeted catalysts **Ir1** and **Ir2**, presumably due to their subcellular localization and positive charge slowing down cellular efflux.

Given that **Ir3'** and **Ir3<sub>mito</sub>** are emissive, we were able to visualize their presence inside live SH-SY5Y cells using fluorescence microscopy (Figure 3B). Cells were treated with 5  $\mu\text{M}$  of an iridium complex for 2 or 24 h and then 10 nM of MitoTracker Deep Red was added for 20 min to stain the mitochondria before imaging. Excitation at 405 nm led to fluorescence (426–450 nm) within the cell interior due to the presence of the pyrene units in **Ir3'** and **Ir3<sub>mito</sub>**. Similarly, excitation at 640 nm resulted in red emission (659–701 nm), showing the location of the mitochondria inside the cells. When the fluorescence images from the 2 h Ir treatment were merged, the Pearson correlation coefficients (PCC) obtained were 0.57 for **Ir3'** and 0.92 for **Ir3<sub>mito</sub>**, which clearly indicate that having the phosphonium group in **Ir3<sub>mito</sub>** is highly effective for targeting the mitochondria. Although **Ir2<sub>mito</sub>** is nonemissive and cannot be tracked in live cells, we expect that it has the same mitochondria-targeting ability based on extensive studies of triphenylphosphonium containing compounds in cells.<sup>23,57</sup>

**Detoxification of External Aldehydes.** We established in previous work that **Ir1** is capable of detoxifying aldehydes in mammalian cells.<sup>52</sup> However, in the interest of achieving greater substrate selectivity, we wondered whether a mitochondria-targeted catalyst would be more efficient at aldehyde detoxification given that mitochondrial respiration is one of the main sources of free radicals responsible for endogenous RASP formation.<sup>21,22,66</sup>

Prior to evaluating the aldehyde detoxification properties of our new Ir complexes, we determined their half-maximal inhibition concentrations ( $\text{IC}_{50}$ ) in SH-SY5Y cells after 24 h treatment. Our data revealed that the iridium species have  $\text{IC}_{50}$  values in the order: **Ir1** (35  $\mu\text{M}$ ) > **Ir3'** (32  $\mu\text{M}$ ) > **Ir3<sub>mito</sub>** (27  $\mu\text{M}$ ) > **Ir2<sub>mito</sub>** (17  $\mu\text{M}$ ) > **Ir2** (10  $\mu\text{M}$ ) (Figure 4A). For comparison, the  $\text{IC}_{50}$  of several conventional detox agents were also measured. We found that Car, sodium ascorbate (Asc), and L-Dopa had low toxicity, with  $\text{IC}_{50}$  values >200  $\mu\text{M}$ . The drug candidate Rep was also well tolerated in SH-SY5Y cells ( $\text{IC}_{50}$  = 101  $\mu\text{M}$ ). Additionally, we confirmed that the aldehyde **Ia** was significantly more cytotoxic than its reduced products **Ib** and **Ic** ( $\text{IC}_{50}$  = 11, 758, and >1000  $\mu\text{M}$  for **Ia**, **Ib**, and **Ic**, respectively). Likewise, the  $\text{IC}_{50}$  value of **IIa** (185  $\mu\text{M}$ ) was lower than that of its corresponding alcohol **IIb** (602  $\mu\text{M}$ ). It should be noted that the lipid-derived **Ia** is more cytotoxic than the dopamine oxidation product **IIa** in SH-SY5Y cells.

In our *in vitro* aldehyde detoxification studies, we first incubated SH-SY5Y cells with a detox agent for 3 h, washed twice with fresh media, and then allowed the cells to grow in the presence of 20  $\mu\text{M}$  of **Ia** for 24 h. Relative to the positive control, which contains cells exposed to only **Ia** without detox agents, treatment with 5  $\mu\text{M}$  of **Ir1**, **Ir2**, **Ir2<sub>mito</sub>**, and **Ir3<sub>mito</sub>** resulted in a 1.3-, 1.7-, 2.1, and 1.8-fold enhancement in cell viability (Figure 4B). Increasing the Ir concentration to 10  $\mu\text{M}$  did not improve its cell protective effects, most likely due to increased toxicity stemming from the Ir complex itself. Lowering the Ir amount to 2.5  $\mu\text{M}$  also did not lead to greater cell survival (Figure S20), suggesting that 5  $\mu\text{M}$  is the optimal treatment concentration. The mitochondria-targeted **Ir2<sub>mito</sub>** was more effective than the nontargeted **Ir2**. Cells that were pretreated with the conventional detox agents Car (1 mM) and L-Dopa (100  $\mu\text{M}$ ) showed greater cell survival (1.3-

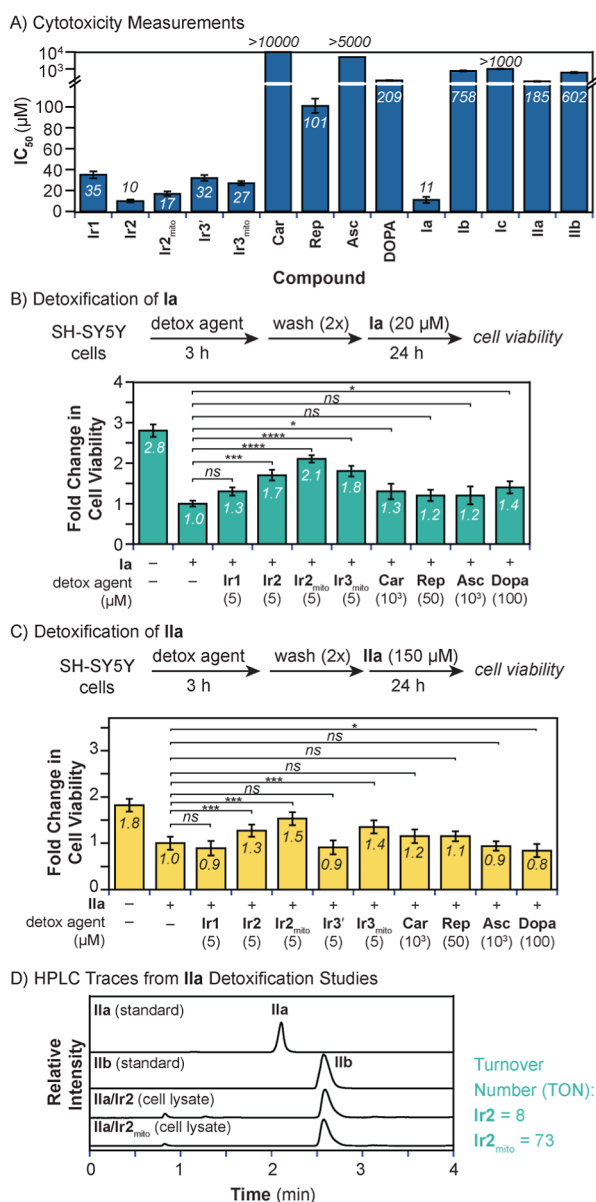


**Figure 4.** (A) The half maximal inhibition concentrations ( $IC_{50}$ ) of various detox agents, aldehydes, and alcohols in SH-SY5Y cells determined using SRB assays after 24 h treatment. (B) Effect of various detox agents on protecting cells against 4-hydroxynon-2-enal (Ia). (C) Effect of various detox agents on protecting cells against 3,4-dihydroxyphenylacetaldehyde (IIa). The fold change in cell viability was calculated as the ratio of the percentage of viable cells in treated wells divided by the percentage of viable cells in control wells containing only aldehydes. The data were analyzed using one-way ANOVA. Data are presented as mean  $\pm$  standard deviation (SD) ( $n = 6$ ). The  $p$ -values are indicated as follows: ns =  $p > 0.05$ , \* =  $p < 0.05$ , \*\* =  $p < 0.01$ , \*\*\* =  $p < 0.001$ , and \*\*\*\* =  $p < 0.0001$ . (D) HPLC traces from IIa detoxification studies.

and 1.4-fold increase, respectively), whereas Rep (50  $\mu$ M) and sodium ascorbate (Asc, 1 mM) resulted in negligible change relative to that in the positive control. These results indicate that Ir2<sub>mito</sub> and Ir3<sub>mito</sub> were most effective at protecting cells from the harmful effects of Ia. Because external aldehydes were added in these experiments, the subcellular location of the Ir catalysts is not likely important for their detoxification abilities. Instead, we hypothesize that the greater biological activity of Ir2<sub>mito</sub> and Ir3<sub>mito</sub> relative to that of Ir1 and Ir2 is due to their

better cellular retention. With regards to the conventional detox agents (i.e., Car, Rep, Asc, and L-Dopa), determining their intracellular concentrations is needed to compare quantitatively their intrinsic detox activity. However, we did not perform such studies because the Ir catalysts were equally or more effective than the conventional detox agents.

Similar detoxification experiments were performed in SH-SY5Y cells using of IIa (150  $\mu$ M) instead of Ia as the substrate (Figure 4C). Because IIa has been implicated in the progression of PD, these studies test the feasibility of catalytic reduction of neurotoxic metabolites. We observed that cells treated with Ir2, Ir2<sub>mito</sub>, and Ir3<sub>mito</sub> improved cell viability by 1.3-, 1.5-, and 1.4-fold, respectively, relative to that in the positive control. Complexes Ir1 and Ir3' did not afford any beneficial effects against IIa, possibly due to their low cell retention after 24 h post-treatment (Figure 3A, right). To confirm that IIa was converted to IIb in the Ir2 and Ir2<sub>mito</sub>-treated samples, we analyzed the cell contents by high performance liquid chromatography (HPLC). The cells were first washed with fresh media, detached from the cell culture plate using trypsin, centrifuged to obtain the cell pellet, and then lysed. The HPLC traces in Figure 4D revealed that cells exposed to IIa and either Ir2 or Ir2<sub>mito</sub>, contained the alcohol IIb, as indicated by the presence of a peak at 2.6 min. By dividing the concentration of IIb by the concentration of iridium in cells determined from the ICP-MS studies above, we obtained turnover numbers (TONs) of 8 for Ir2 and 73 for Ir2<sub>mito</sub> (Table S3). These results indicate that the iridium complexes are capable of catalytic turnover inside living cells. As a control, treatment of cells with IIa (200  $\mu$ M) without any Ir complex did not yield detectable amounts of IIb (Figure S25A). Finally, it should be noted that none of the conventional detox agents (e.g., Car, Rep, Asc, and L-Dopa) provided statistically significant protection against IIa (Figure 4C).

**Protection of MPP<sup>+</sup>-Inhibited Cells.** To explore the possible effects of detox agents on PD, we performed experiments on SH-SY5Y cells treated with 1-methyl-4-phenylpyridinium iodide (MPP<sup>+</sup>), which interferes with oxidative phosphorylation by inhibiting Complex I in the mitochondria and induces Parkinsonism on the cellular level.<sup>67–71</sup> First, we evaluated the toxicity of MPP<sup>+</sup> in SH-SY5Y cells and observed a concentration- and time-dependent reduction in cell viability (Figure S27). Next, cells were incubated with a detox agent for 3 h, washed twice with fresh media, and then exposed to 1 mM of MPP<sup>+</sup> for 24 h (Figure 5A). Cells that were treated with only MPP<sup>+</sup> without detox agents showed decreased viability (54%) relative to that in the untreated group (Figure S28). Preincubation with the Ir complexes improved cell survival in nearly all cases. For example, the presence of Ir2 and Ir2<sub>mito</sub> increased viability by 1.2- and 1.3-fold relative to that in the positive control, respectively (Figure 5A). The addition of sodium formate (1 mM), as an external hydride source, did not enhance the effects of the Ir complexes by an appreciable amount.

For comparison, similar studies were conducted using conventional detox agents. Our results indicated that Car (1 mM), Rep (50  $\mu$ M), Asc (1 mM), and L-Dopa (50  $\mu$ M) had mild to moderate effects, resulting in 1.2-, 1.3-, 1.1-, and 1.2-fold increase in cell viability relative to that in the positive control (Figure 5A). It is important to note that the amounts of conventional detox agents used in these experiments were 5–200 $\times$  higher than that of the Ir catalysts since their  $IC_{50}$

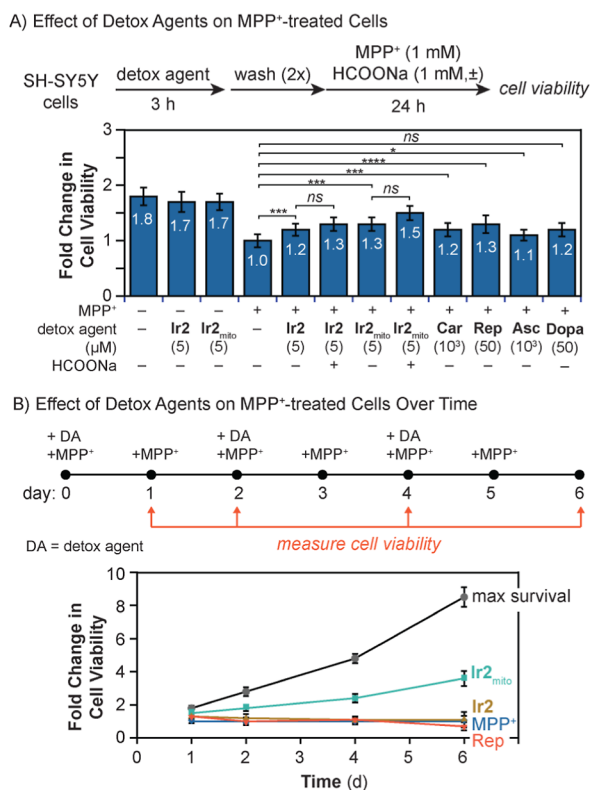


**Figure 5.** (A) Studies of detox agents on their ability to protect SH-SY5Y cells against MPP<sup>+</sup>-induced cell death (24 h). (B) Comparison of the effects of detox agents over the course of 6 days (see Figures S30 and S31 for the full data set). The fold change in cell viability was calculated as the ratio of the percentage of viable cells in treated wells divided by the percentage of viable cells in control wells containing only aldehydes. The data were analyzed using one-way ANOVA. Data are presented as mean  $\pm$  standard deviation (SD) ( $n = 6$ ). The  $p$ -values are indicated as follows: ns =  $p > 0.05$ , \* =  $p < 0.05$ , \*\* =  $p < 0.01$ ; \*\*\* =  $p < 0.001$ , and \*\*\*\* =  $p < 0.0001$ .

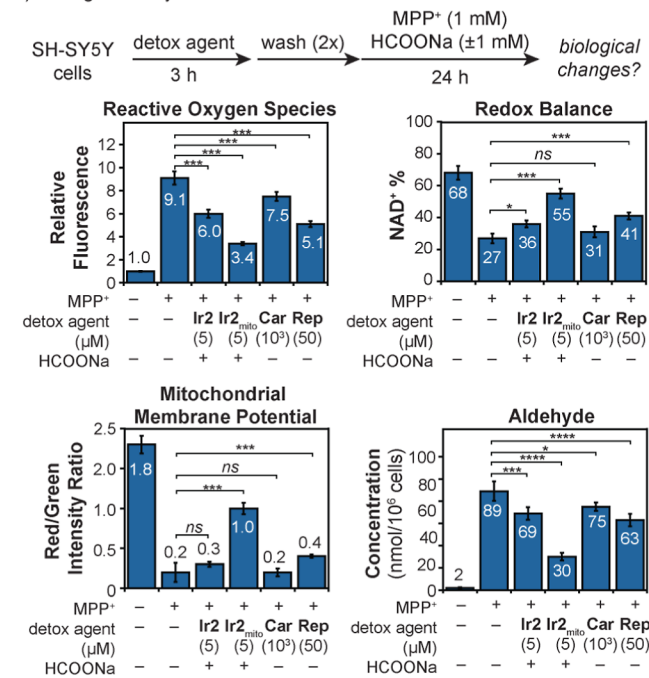
values are greater (Figure 4A). Once again, our data indicate that the Ir complexes were just as or more effective than the conventional detox agents.

Because catalysts can turnover reactions continuously until they deactivate, it has the potential to exhibit longer-lasting effects than stoichiometric reactants. To explore this possibility, we performed detoxification studies over the course of multiple days. The SH-SY5Y cells were combined with a detox agent for 3 h, washed twice with fresh media, and then incubated with MPP<sup>+</sup> for 21 h (day 1). Subsequently, cells were treated with MPP<sup>+</sup> each day (on days 2–5) whereas additional detox agents were added every other day (on days 2 and 4). On day 6, the cell viability was measured (Figures 5B, S30 and S31). We observed that while all the detox agents showed some protective effects after day 1, only Ir<sub>2</sub><sub>mito</sub> and Ir<sub>3</sub><sub>mito</sub> (see Figure S30 for Ir<sub>3</sub><sub>mito</sub> results) were capable of increasing cell viability up to day 6. We hypothesize that the subcellular localization and better cell retention of the mitochondria-targeted catalysts enable them to amplify their catalytic mechanism of action over a longer period than nontargeted or stoichiometric detox agents.

**Changes to Key Biomarkers.** Given the promising results above, we investigated the impact of various detox agents on key biomarkers in the MPP<sup>+</sup>-inhibited cells. A fluorometric assay based on 2,7-dichlorofluorescein diacetate was used to

quantify intracellular ROS (Figure S35). As expected, cells treated with only MPP<sup>+</sup> displayed significantly higher levels of ROS (9.1 $\times$ ) relative to that in the untreated control (Figure 6A, upper left). Catalyst Ir<sub>2</sub><sub>mito</sub> (3.4 $\times$ ) suppressed the ROS concentration to a greater extent than Ir<sub>2</sub> (6.0 $\times$ ), Car (7.5 $\times$ ), and Rep (5.1 $\times$ ).

#### A) Changes to Key Biomarkers



#### B) Summary of Biological Effects

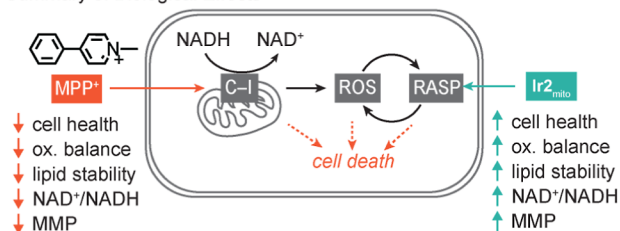


**Figure 6.** (A) Comparing the effects of various detox agents on key biomarkers, including reactive oxygen species, redox balance, mitochondrial membrane potential (MMP), and aldehyde concentration. (B) A scheme showing the cell protective properties of Ir<sub>2</sub><sub>mito</sub> against MPP<sup>+</sup>-induced cytotoxicity. C-I = Complex I of the mitochondrial respiration system.

Given that MPP<sup>+</sup> interferes with Complex I in the mitochondria, which catalyzes the transfer of electrons from NADH to coenzyme Q, the percentage of NAD<sup>+</sup> (the oxidized form of NADH) in cells is expected to decrease.<sup>68,71</sup> To measure the [NAD<sup>+</sup>]/[NADH] ratio, a commercial colorimetric assay was used (Figure S37). We found that MPP<sup>+</sup> inhibition lowered the intracellular NAD<sup>+</sup> content to 27% from 68% in the negative control. Treatment with Ir<sub>2</sub>, Ir<sub>2</sub><sub>mito</sub>, and Rep gave NAD<sup>+</sup> amounts of 36, 55, and 41%, respectively. In contrast, Car had a negligible effect on the NAD<sup>+</sup>% (Figure 6A, upper right).

To assess the impact of MPP<sup>+</sup> on the mitochondria integrity, the mitochondrial membrane potential (MMP) was quantified using a commercial JC-10 assay (Figure S36). In these experiments, a higher ratio of red/green fluorescence is

indicative of normal mitochondria health and vice versa. Our measurements indicated that the red/green ratio in the positive control is 0.2, which is consistent with the role of MPP<sup>+</sup> as a mitochondrial inhibitor.<sup>68</sup> Among the detox agents tested, only Ir2<sub>mito</sub> (red/green = 1.0) and Rep (red/green = 0.4) had beneficial effects on the MMP (Figure 6A, bottom left). Complex Ir2<sub>mito</sub> had a more pronounced effect than Ir2 on all the cellular biomarkers above, suggesting that mitochondria-targeting is a beneficial design feature.<sup>71</sup>

To explore the possibility of RASP detoxification in the PD cell models, we also quantified the amounts of aldehydes present in each treatment group (Figure S38). The commercial assay used is nonspecific, so it can detect a variety of RASP, such as Ia, acrolein, malondialdehyde, and others. We observed that in the MPP<sup>+</sup> treated cells, the aldehyde concentration was 89 nmol/10<sup>6</sup> cells, which was about 44× higher than that in untreated cells (Figure 6A, bottom right). Although all the detox agents decreased the amounts of aldehydes observed compared to that in the positive control, the use of Ir2<sub>mito</sub> and HCOONa was the most successful (i.e., lowered aldehyde levels to 30 nmol/10<sup>6</sup> cells). To estimate the TON of the iridium catalysts, we assumed that the quantity of aldehydes generated is 89 nmol/10<sup>6</sup> cells in all MPP<sup>+</sup>-inhibited cells. The actual amount is likely lower since less ROS should lead to lower lipid peroxidation so our calculated numbers are upper limits. By dividing the amount of aldehyde converted by the amount of Ir catalysts in the cells, we obtained TONs of 59 for Ir2 and 536 for Ir2<sub>mito</sub> (Figure S39). To the best of our knowledge, this study is the first to demonstrate catalytic turnover of endogenously produced RASP by nonenzymatic catalysis.

The results from our study are summarized in Figure 6B. It is well established that MPP<sup>+</sup> induces Parkinsonism by inhibiting mitochondrial respiration and lowering the cellular redox balance, lipid stability, NAD<sup>+</sup>/NADH ratio, and MMP.<sup>67–71</sup> High concentrations of intracellular ROS can promote lipid degradation into RASP, which can disrupt biological systems by alkylating biomolecules or cross-linking proteins.<sup>44</sup> These processes ultimately lead to dopaminergic cell death in PD. Based on our biochemical measurements, treating cells with our mitochondria-targeted Ir catalysts reversed many of the biomarkers associated with Parkinsonism. Our studies suggest that the Ir detox agents do not intervene in MPP<sup>+</sup> inhibition but rather, they minimize the downstream effects that cause further cellular damage. For example, the Ir complexes could lower the RASP burden by converting them into nontoxic alcohols, which presumably would lead to decreased ROS and oxidative stress. Consistent with previous reports,<sup>72</sup> additional experiments demonstrated that treatment of SH-SY5Y cells with Ia significantly increased ROS levels (Figure S35), further supporting our hypothesis. It is possible that the cationic forms of the Ir complexes could compete for the same bindings sites as MPP<sup>+</sup> at C–I of the mitochondria. However, further studies are needed to interrogate such interactions as well as explore other possible modes of action (e.g., reduction of NAD<sup>+</sup> and/or CoQ10<sup>73,74</sup> by the Ir complexes and HCOONa).

Because the root cause of PD is still unknown, having diverse strategies to mitigate its progression may be the best therapeutic approach. Although significant research in PD has focused on controlling neurotransmitter levels in the brain, our work suggests that targeting mitochondria dysfunction via catalytic RASP detoxification could offer additional benefits.

To advance our research on catalytic detox agents, studies are needed to investigate their BBB permeability and absorption, distribution, metabolism, excretion, and toxicity in vivo.<sup>75,76</sup> In preliminary studies using a Parallel Artificial Membrane Permeability Assay (PAMPA), we found that complexes Ir1, Ir2<sub>mito</sub>, and Ir3' have high cell membrane permeability (Table S5).<sup>77</sup> However, only Ir1 and Ir2<sub>mito</sub> were predicted to be capable of crossing the BBB via passive diffusion, as indicated by their permeability coefficient ( $P_e$ ) of  $>4 \times 10^{-6}$  cm/s.<sup>78,79</sup>

Finally, the Ir complexes must also be tested in various models of neurodegeneration to assess their potential clinical relevance. The use of metal complexes to interfere with toxic protein aggregation has shown promise in solution, cellular, and animal models.<sup>80–83</sup>

## CONCLUSIONS

We have prepared a new series of organoiridium complexes as catalytic detox agents against biogenic RASP. We demonstrated that the Ir complexes bearing phosphonium groups colocalize in the mitochondria of SH-SY5Y cells and have greater cell retention compared to that of their parent Ir complex. Studies in solution and inside living cells showed that our catalysts can efficiently convert the neurotoxic metabolite Ia into the corresponding nontoxic alcohol with catalytic turnover. To simulate Parkinsonism on the cellular level, SH-SY5Y cells were exposed to MPP<sup>+</sup>, which decreased oxidative balance, lipid stability, NAD<sup>+</sup>/NADH ratio, and MMP relative to that of normal cells. Although both Ir and organic detox agents provided some degree of cellular protection, the mitochondria-targeted Ir complexes exhibited the longest-lasting effects of up to 6 d. Our data suggest that the Ir detox agents had TONs as high as 536 for the conversion of endogenously generated RASP. The results presented here make a compelling case for considering Ir detox agents as possible therapeutics for PD. However, as is the case for any compounds to be considered for clinical applications, further studies of their BBB permeability and biological effects in various in vitro and in vivo models need to be evaluated. Nevertheless, this research demonstrates that catalytic detox agents have unique benefits over conventional stoichiometric agents and offers a new therapeutic strategy to consider in advanced drug discovery programs.

## EXPERIMENTAL SECTION

**General Procedures.** All chemicals and reagents were purchased from commercial sources and were used without further purification unless otherwise noted. All air- and water-sensitive manipulations were performed using standard Schlenk techniques or under a nitrogen atmosphere using a glovebox. Anhydrous solvents were obtained from an Innovative Technology solvent drying system saturated with Argon. The purity of all compounds used was determined by NMR spectroscopy to be >95% pure. Synthetic procedures of compounds 2, 3, 5, 6, 7, 12, 13, 14, 15, and 16 are provided in the Supporting Information. SH-SY5Y cell lines were obtained commercially from the American Type Culture Collection (ATCC). Procedures for the PAMPA are given in the Supporting Information.

**Physical Methods.** NMR spectra were acquired using JEOL spectrometers (ECA-400, 500, and 600) at room temperature and referenced using residual solvent peaks. All <sup>13</sup>C NMR spectra were proton decoupled. High-resolution mass spectra were obtained at the University of Texas-Austin Mass Spectrometry Facility using an Agilent 6546 Q-TOF LC/MS. Gas chromatography–mass spectrometry (GC–MS) was performed using an Agilent 7890 GC/5977A MSD instrument equipped with an HP-5MS capillary column. For the

temperature program used for GC–MS analysis, samples were held at 60 °C for 3 min, heated from 60 to 280 °C at 10 °C/min, and then held at 280 °C for 3 min. The inlet temperature was set constant at 280 °C. The GC–MS spectra obtained were compared with those in the NIST library. Infrared (IR) spectra were measured by using a Thermo Nicolet Avatar FTIR spectrometer with a diamond ATR. Ultraviolet–visible (UV–vis) absorption spectroscopic studies were performed using an Agilent Cary 60 spectrophotometer. Electrolyte composition was tested by solution-mode ICP–MS applying an Agilent 7500ce with a collision reaction cell (He and H<sub>2</sub> modes, The University of Texas Jackson School of Geosciences). A Tecan Infinite M200 Pro plate reader was used to measure the absorbance and fluorescence intensity in cellular studies. All biological cell images were obtained using an Olympus IX83 microscope equipped with a 100× oil-immersion objective.

**Synthesis and Characterization. Preparation of L2.** In a 100 mL round-bottom flask, 2-picolinic acid (1.58 g, 10.0 mmol, 1.0 equiv) was dissolved in ~30 mL of anhydrous dichloromethane and cooled in an ice bath for ~15 min. Triethylamine (4.18 mL, 30.0 mmol, 3.0 equiv) was added to the reaction mixture and stirred for 15 min. The mixture was then treated with ethyl chloroformate (1.24 mL, 13.0 mmol, 1.3 equiv) and stirred in an ice bath for another 30 min before combining with decylamine (0.94 g, 6.0 mmol, 0.6 equiv). The reaction was stirred in an ice bath for 1 h, warmed to 25 °C, and stirred for another 24 h. Once the reaction was complete, water was added and the organic phase was separated, dried over sodium sulfate, filtered to remove the drying agent, and evaporated to dryness. The crude product was purified by silica gel column chromatography (20% ethyl acetate in hexane) to obtain a colorless oil (695 mg, 44% yield). <sup>1</sup>H NMR (CDCl<sub>3</sub>, 500 MHz): δ 8.54 (d, *J* = 4.3 Hz, 1H), 8.20 (d, *J* = 7.8 Hz, 1H), 8.05 (s, 1H), 7.84 (td, *J* = 7.7, 1.6 Hz, 1H), 7.42 (ddd, *J* = 7.5, 4.8, 1.0 Hz, 1H), 3.46 (q, *J* = 7.0 Hz, 2H), 1.63 (q, *J* = 7.5 Hz, 2H), 1.45–1.19 (m, 14H), and 0.87 (t, *J* = 6.9 Hz, 3H) ppm. <sup>13</sup>C NMR (CDCl<sub>3</sub>, 151 MHz): δ 164.27, 150.18, 148.08, 137.43, 126.11, 122.28, 39.57, 31.99, 29.76, 29.64, 29.44, 29.41, 29.39, 27.12, 22.78, and 14.22 ppm. HRMS ESI(+): calcd for C<sub>16</sub>H<sub>26</sub>N<sub>2</sub>O<sub>2</sub>Na *m/z* = 285.1943 [M + Na]<sup>+</sup>, found *m/z* = 285.1953.

**Preparation of Ir2.** In a 50 mL Schlenk flask, 20 mL of dichloromethane was purged with nitrogen for about 10 min. [Cp\*IrCl<sub>2</sub>]<sub>2</sub> (189.5 mg, 0.237 mmol, 1.0 equiv) and ligand L2 (125 mg, 0.475 mmol, 2.0 equiv) were added and stirred for 5 min at 25 °C. The reaction mixture was then treated with NEt<sub>3</sub> (66 μL, 0.933 mmol, 2.0 equiv) and stirred for another 24 h at 25 °C. Once the reaction was complete, the reaction mixture was washed with water (3 × 20 mL). The organic phase was separated, dried over sodium sulfate, filtered to remove the drying agent, and then evaporated to dryness. The crude product was purified by silica gel column chromatography (5% methanol in ethyl acetate) to obtain a yellow solid (204 mg, 68% yield). <sup>1</sup>H NMR (CDCl<sub>3</sub>, 400 MHz): δ 8.50 (d, *J* = 5.2 Hz, 1H), 8.09–8.03 (m, 1H), 7.86 (td, *J* = 7.7, 1.2 Hz, 1H), 7.43–7.36 (m, 1H), 4.57 (ddd, *J* = 12.0, 10.1, 6.6 Hz, 1H), 3.20–2.97 (m, 1H), 1.66 (s, 15H), 1.34 (dd, *J* = 35.5, 6.2 Hz, 4H), 1.24 (s, 12H), and 0.86 (t, *J* = 6.9 Hz, 3H) ppm. <sup>13</sup>C NMR (CDCl<sub>3</sub>, 126 MHz): δ 169.89, 156.03, 148.91, 138.42, 126.70, 125.98, 86.39, 50.48, 32.03, 29.92, 29.83, 29.75, 29.45, 29.32, 27.89, 22.78, 14.23, and 8.91 ppm. IR (ν̄): 2921, 2852, 1619, 1591, 1563, 1466, 1381, 1288, 1029, 763, 685, and 504 cm<sup>-1</sup>. HRMS ESI(+): calcd for C<sub>26</sub>H<sub>41</sub>ClIrN<sub>2</sub>O *m/z* = 625.2537 [M + H]<sup>+</sup>, found *m/z* = 625.2520.

**Preparation of L2<sub>mito</sub>.** In a 100 mL round-bottom flask, 2-picolinic acid (198 mg, 1.61 mmol, 1.0 equiv) was dissolved in ~25 mL of anhydrous dichloromethane and cooled in an ice bath for ~10 min. Triethylamine (645 μL, 4.85 mmol, 3.0 equiv) was added to the reaction solution and stirred for 15 min. The mixture was then treated with ethyl chloroformate (200 μL, 2.09 mmol, 1.3 equiv) and stirred in an ice bath for another 30 min before combining with compound 3 (482 mg, 0.97 mmol, 0.6 equiv.; see Supporting Information for structure). The reaction was stirred in an ice bath for 1 h, warmed to 25 °C, and stirred for another 24 h. Once the reaction was complete, water was added and the organic phase was separated, dried over sodium sulfate, filtered to remove the drying agent, and evaporated to

dryness. The crude product was purified by silica gel column chromatography (10% methanol in dichloromethane) to afford a white solid (221.8 mg, 38% yield). <sup>1</sup>H NMR (CDCl<sub>3</sub>, 400 MHz): δ 8.54 (d, *J* = 4.4 Hz, 1H), 8.17 (d, *J* = 7.8 Hz, 1H), 8.07 (s, 1H), 7.90–7.66 (m, 16H), 7.41 (dd, *J* = 7.0, 4.9 Hz, 1H), 3.77 (s, 2H), 3.42 (q, *J* = 6.8 Hz, 2H), 2.03 (m, 2H), 1.59 (m, *J* = 6.0 Hz, 6H), and 1.21 (m, *J* = 20.1 Hz, 8H) ppm. <sup>13</sup>C NMR (CDCl<sub>3</sub>, 151 MHz): δ 164.36, 150.09, 148.19, 137.47, 135.03, 133.92, 133.89, 130.61, 126.20, 122.24, 118.67, 39.53, 30.49, 29.73, 29.42, 29.25, 29.17, 27.00, and 22.76 ppm. <sup>13</sup>P NMR (CDCl<sub>3</sub>, 162 MHz): δ 25.12 ppm.

**Preparation of Ir2<sub>mito</sub>.** In a 50 mL Schlenk flask, 15 mL of dichloromethane was purged with nitrogen for about 10 min. [Cp\*IrCl<sub>2</sub>]<sub>2</sub> (36 mg, 0.045 mmol, 1.0 equiv) and ligand L2<sub>mito</sub> (54.7 mg, 0.091 mmol, 2.0 equiv) were added and stirred for 5 min at 25 °C. The reaction mixture was then treated with Et<sub>3</sub>N (13 μL, 0.091 mmol, 2.0 equiv) and stirred under reflux for another 24 h. Once the reaction was complete, the reaction mixture was washed with water (3 × 20 mL). The organic phase was separated, dried over sodium sulfate, filtered to remove the drying agent, and then evaporated to dryness. The crude product was purified by silica gel column chromatography (10% methanol in dichloromethane) to obtain a yellow solid (57 mg, 66% yield). <sup>1</sup>H NMR (CDCl<sub>3</sub>, 400 MHz): δ 8.51 (d, *J* = 5.5 Hz, 1H), 7.99 (d, *J* = 7.8 Hz, 1H), 7.87–7.77 (m, 10H), 7.70 (td, *J* = 7.8, 3.4 Hz, 6H), 7.42 (t, *J* = 6.5 Hz, 1H), 4.65–4.41 (m, 1H), 3.79–3.55 (m, 2H), 3.05 (td, *J* = 11.6, 4.6 Hz, 1H), 1.90 (m, 4H), 1.65 (s, 15H), 1.60–1.52 (m, 4H), and 1.30–1.08 (m, 8H) ppm. <sup>13</sup>C NMR (CDCl<sub>3</sub>, 101 MHz): δ 169.96, 155.97, 149.02, 138.46, 135.18, 133.72, 130.68, 126.38, 118.47, 86.50, 50.35, 30.28, 29.29, 28.87, 27.63, 22.52, and 8.99 ppm. <sup>13</sup>P NMR (CDCl<sub>3</sub>, 202 MHz): δ 24.68 ppm. IR (ν̄): 2923, 2852, 1616, 1588, 1562, 1438, 1395, 1112, 1028, 752, 723, 687, 532, and 505 cm<sup>-1</sup>. HRMS ESI(+): calcd for C<sub>44</sub>H<sub>54</sub>ClIrN<sub>2</sub>OP *m/z* = 885.3286 [M–Br]<sup>+</sup>, found *m/z* = 885.3262.

**Preparation of L3<sub>mito</sub>.** Compound 7 (173 mg, 0.508 mmol, 1.0 equiv) and diphenyl(1-pyrenyl)phosphine (216 mg, 0.559 mmol, 1.1 equiv) were dissolved in 20 mL of dry THF in a high-pressure glass tube and the mixture was stirred at 130 °C for 72 h. After the reaction was complete, the solvent was removed under vacuum and the crude product was purified by silica column chromatography (8% methanol in dichloromethane) to obtain an off-white solid (118 mg, 32% yield). <sup>1</sup>H NMR (CDCl<sub>3</sub>, 400 MHz): δ 8.57 (m, 1H), 8.47–8.40 (m, 2H), 8.37 (dd, *J* = 8.3, 6.3 Hz, 2H), 8.32–8.16 (m, 6H), 7.95–7.79 (m, 8H), 7.73 (m, 4H), 7.48 (m, 1H), 3.71 (m, 2H), 3.42 (q, *J* = 6.7 Hz, 2H), 1.59–1.53 (m, 4H), 1.30–1.24 (m, 4H), and 1.23–1.11 (m, 8H) ppm. <sup>13</sup>C NMR (CDCl<sub>3</sub>, 151 MHz): δ 164.31, 150.13, 148.15, 137.45, 136.65, 136.63, 134.90, 133.93, 133.63, 133.13, 132.03, 131.21, 131.07, 130.72, 129.90, 128.24, 127.66, 126.17, 125.67, 125.40, 123.84, 122.22, 119.91, 108.28, 107.99, 39.49, 30.50, 29.64, 29.24, 29.05, 26.92, 24.97, and 23.76 ppm. <sup>13</sup>P NMR (CDCl<sub>3</sub>, 162 MHz): δ 24.67 ppm. HRMS ESI(+): calcd for C<sub>44</sub>H<sub>44</sub>N<sub>2</sub>OP *m/z* = 647.3186 [M–Br]<sup>+</sup>, found *m/z* = 647.3189.

**Preparation of Ir3<sub>mito</sub>.** In a 50 mL Schlenk flask, 15 mL of dichloromethane was purged with nitrogen for about 10 min. [Cp\*IrCl<sub>2</sub>]<sub>2</sub> (39 mg, 0.048 mmol, 0.7 equiv) and ligand L3<sub>mito</sub> (50 mg, 0.069 mmol, 1.0 equiv) were added and stirred for 5 min at 25 °C. The reaction mixture was then treated with NEt<sub>3</sub> (10 μL, 0.091 mmol, 1.0 equiv) and stirred under reflux for another 24 h. Once the reaction was complete, the reaction mixture was washed with water (3 × 20 mL). The organic phase was separated, dried over sodium sulfate, and then evaporated to dryness. The crude product was purified by silica gel column chromatography (10% methanol in dichloromethane) to obtain a yellow solid (51 mg, 68% yield). <sup>1</sup>H NMR (CDCl<sub>3</sub>, 600 MHz): δ 8.50 (d, *J* = 4.7 Hz, 1H), 8.47–8.38 (m, 2H), 8.38–8.33 (m, 2H), 8.29 (dd, *J* = 14.4, 8.1 Hz, 1H), 8.22 (d, *J* = 8.9 Hz, 1H), 8.16 (dd, *J* = 8.3, 7.2 Hz, 2H), 7.99 (d, *J* = 7.6 Hz, 1H), 7.94–7.76 (m, 8H), 7.41 (ddd, *J* = 7.3, 5.5, 1.6 Hz, 1H), 4.51 (m, 1H), 3.82 (m, 2H), 3.03 (m, 1H), 1.79 (m, 6H), 1.64 (s, 15H), 1.53 (d, *J* = 8.4 Hz, 2H), 1.25 (m, 2H), and 1.17–1.01 (m, 8H) ppm. <sup>13</sup>C NMR (CDCl<sub>3</sub>, 126 MHz): δ 169.97, 156.04, 149.03, 138.42, 135.06, 135.03, 133.54, 133.46, 133.00, 132.91, 132.10, 131.27, 130.85,

130.75, 129.92, 128.35, 128.27, 127.70, 127.31, 126.82, 125.91, 125.77, 125.66, 123.61, 123.55, 86.50, 50.35, 30.41, 29.83, 29.37, 28.84, 27.59, 25.02, 24.62, 23.62, and 8.99 ppm.  $^{13}\text{P}$  NMR ( $\text{CDCl}_3$ , 162 MHz):  $\delta$  24.63 ppm. IR ( $\bar{\nu}$ ): 2923, 2852, 1616, 1589, 1563, 1438, 1381, 1260, 1209, 1106, 1029, 858, 800, 751, 716, 686, 633, 596, and 582  $\text{cm}^{-1}$ . HRMS ESI(+): calcd for  $\text{C}_{54}\text{H}_{58}\text{ClIrN}_2\text{OP}$   $m/z$  = 1009.3599  $[\text{M}-\text{Br}]^+$ , found  $m/z$  = 1009.3580.

**Preparation of tert-Butyl (4-Oxo-4-(pyren-1-ylmethyl)amino)-butyl)carbamate (9).** In a 100 mL round-bottom flask, Boc-GABA-OH (**8**) (364 mg, 1.8 mmol) was dissolved in a mixture of  $\text{CH}_2\text{Cl}_2$ /DMF (1:1) (40 mL). Then, *N,N*-diisopropylethylamine (DIPEA, 0.8 mL, 4.5 mmol) was introduced into the solution, and the resulting mixture was stirred at room temperature for 30 min. After 30 min, EDC-HCl (430 mg, 2.24 mmol) and 1-pyrenemethylamine hydrochloride (400 mg, 1.5 mmol) were added to the reaction flask and then heated at 50 °C for an additional 24 h. Upon completion of the reaction, the reaction mixture was slowly poured into water (25 mL) and the resulting solution was extracted with  $\text{CH}_2\text{Cl}_2$  (30 mL). The organic phase was washed with water (3 $\times$ ) and then evaporated to dryness. The crude product was purified by silica gel column chromatography (80% ethyl acetate in hexane) to obtain a light-yellow solid (425 mg, 69%).  $^1\text{H}$  NMR ( $\text{CDCl}_3$ , 400 MHz):  $\delta$  8.11–8.08 (m, 3H), 8.02 (d,  $J$  = 8.1 Hz, 2H), 7.98–7.90 (m, 3H), 7.83 (d,  $J$  = 7.8 Hz, 1H), 6.70 (s, 1H), 4.97 (d,  $J$  = 5.3 Hz, 2H), 4.87 (m, 1H), 3.06 (q,  $J$  = 6.2 Hz, 2H), 2.15 (t,  $J$  = 7.0 Hz, 2H), 1.75 (p,  $J$  = 6.8 Hz, 2H), and 1.37 (s, 9H) ppm.  $^{13}\text{C}$  NMR ( $\text{CDCl}_3$ , 126 MHz):  $\delta$  172.36, 156.56, 131.34, 131.27, 130.86, 129.09, 128.27, 127.59, 127.47, 127.32, 126.18, 125.47, 125.42, 125.11, 124.89, 124.82, 123.02, 79.47, 42.05, 39.85, 33.76, 28.46, and 26.53 ppm.

**Preparation of 4-Amino-N-(pyren-1-ylmethyl)butanamide (10).** In a 50 mL round-bottom flask, compound **9** (425 mg, 1.02 mmol) was dissolved in a 15% (v/v) solution of  $\text{CF}_3\text{CO}_2\text{H}$  in  $\text{CH}_2\text{Cl}_2$  (20 mL) at 0 °C. The reaction mixture was stirred for 10 min at 0 °C. The resulting solution was allowed to warm up to 25 °C and stirred for an additional 4 h. Once the reaction was complete, the solvent was evaporated to dryness, and the crude product was purified by silica gel column chromatography (10–15% of  $\text{CH}_3\text{OH}$  in  $\text{CH}_2\text{Cl}_2$ ) to obtain the desired product as a yellow solid (310 mg, 96%).  $^1\text{H}$  NMR ( $\text{CD}_3\text{OD}$ , 600 MHz):  $\delta$  6.63 (d,  $J$  = 9.2 Hz, 1H), 6.56 (dd,  $J$  = 7.5, 3.5 Hz, 2H), 6.50 (t,  $J$  = 9.3 Hz, 2H), 6.43–6.32 (m, 4H), 3.44 (s, 2H), 1.70 (s, 1H), 1.34 (t,  $J$  = 7.5 Hz, 2H), 0.79 (t,  $J$  = 7.1 Hz, 2H), and 0.35 (p,  $J$  = 7.2 Hz, 2H) ppm.  $^{13}\text{C}$  NMR ( $\text{CD}_3\text{OD}$ , 151 MHz):  $\delta$  174.08, 132.71, 132.25, 130.02, 128.90, 128.38, 128.10, 127.17, 126.37, 126.33, 126.05, 125.79, 123.91, 42.46, 40.37, 33.70, and 24.56 ppm.

**Preparation of L3'.** In a 100 mL round-bottom flask, 2-picolinic acid (156 mg, 1.27 mmol) was dissolved in a mixture of  $\text{CH}_2\text{Cl}_2$ /DMF (1:1) (40 mL). *N,N*-Diisopropylethylamine (DIPEA, 0.51 mL, 2.94 mmol) was added into the solution, and the resulting reaction mixture was then stirred at room temperature for 30 min. After 30 min, EDC-HCl (319 mg, 1.67 mmol) and compound **10** (310 mg, 0.98 mmol; see [Supporting Information](#) for structure) were introduced into the reaction flask and heated at 50 °C for an additional 24 h. Once the reaction was complete, the reaction mixture was slowly poured into water (25 mL), and the resulting solution was extracted with  $\text{CH}_2\text{Cl}_2$  (30 mL). The organic phase was washed with water (3 $\times$ ) and then evaporated to dryness. The crude product was purified by silica gel column chromatography (5% methanol in ethyl acetate) to obtain a light-yellow solid (100 mg, 24%).  $^1\text{H}$  NMR ( $\text{CDCl}_3$ , 600 MHz):  $\delta$  8.42 (dd,  $J$  = 4.8, 1.5 Hz, 1H), 8.20 (d,  $J$  = 9.1 Hz, 1H), 8.16 (t,  $J$  = 6.4 Hz, 1H), 8.13 (dd,  $J$  = 7.9, 2.8 Hz, 2H), 8.08–8.03 (m, 2H), 8.02–7.94 (m, 4H), 7.90 (d,  $J$  = 7.5 Hz, 1H), 7.66 (td,  $J$  = 7.7, 1.9 Hz, 1H), 7.29 (m, 1H), 6.82 (t,  $J$  = 5.6 Hz, 1H), 5.07 (d,  $J$  = 5.3 Hz, 2H), 3.44 (q,  $J$  = 6.7 Hz, 2H), 2.27 (t,  $J$  = 7.1 Hz, 2H), and 1.96 (p,  $J$  = 6.9 Hz, 2H) ppm.  $^{13}\text{C}$  NMR ( $\text{CDCl}_3$ , 151 MHz):  $\delta$  172.25, 164.83, 149.52, 148.02, 137.21, 131.39, 131.21, 131.05, 130.73, 128.94, 128.05, 127.37, 127.17, 126.12, 126.03, 125.28, 124.93, 124.76, 124.68, 122.97, 122.04, 77.34, 77.13, 76.92, 41.88, 38.72, 33.79, and 26.13 ppm. HRMS ESI(+): calculated for  $\text{C}_{27}\text{H}_{23}\text{N}_3\text{O}_2\text{Na}$   $m/z$  = 444.1688  $[\text{M} + \text{Na}]^+$ , found  $m/z$  = 444.1674.

**Preparation of Ir3'.** In a 50 mL Schlenk flask, 15 mL of dichloromethane was purged with nitrogen for about 10 min.  $[\text{Cp}^*\text{IrCl}_2]_2$  (58 mg, 0.072 mmol, 0.6 equiv) and ligand **L3'** (50 mg, 0.12 mmol, 1.0 equiv) were added and stirred for 5 min at 25 °C. The reaction mixture was then treated with  $\text{NEt}_3$  (25  $\mu\text{L}$ , 0.18 mmol, 1.5 equiv) and stirred for another 24 h at 25 °C. Once the reaction was complete, the reaction mixture was washed with water (3  $\times$  15 mL). The organic phase was separated, dried over sodium sulfate, filtered to remove the drying agent, and then evaporated to dryness. The crude product was purified by silica gel column chromatography (10% methanol in dichloromethane) to obtain a yellowish-brown solid (68 mg, 72% yield).  $^1\text{H}$  NMR ( $\text{CDCl}_3$ , 600 MHz):  $\delta$  8.37–8.30 (m, 2H), 8.17–8.11 (m, 2H), 8.12–8.06 (m, 3H), 8.05–7.90 (m, 5H), 7.77 (t,  $J$  = 7.6 Hz, 1H), 7.32 (t,  $J$  = 6.5 Hz, 1H), 5.37 (dd,  $J$  = 14.7, 6.8 Hz, 1H), 4.91 (dd,  $J$  = 14.7, 4.2 Hz, 1H), 4.70–4.59 (m, 1H), 3.11–2.97 (m, 1H), 2.30–2.35 (m, 1H), 2.26–2.19 (m, 1H), 1.99–1.84 (m, 2H), and 1.28 (s, 15H) ppm.  $^{13}\text{C}$  NMR ( $\text{CDCl}_3$ , 151 MHz):  $\delta$  174.36, 170.98, 155.51, 148.89, 138.57, 132.91, 131.33, 130.90, 128.96, 127.61, 127.19, 127.00, 126.00, 125.04, 124.93, 123.86, 86.31, 47.36, 41.54, 34.77, 27.27, and 8.47 ppm. IR ( $\bar{\nu}$ ): 2921, 1647, 1617, 1587, 1562, 1439, 1377, 1260, 1183, 1095, 1026, 848, 761, 707, 684, and 504  $\text{cm}^{-1}$ . HRMS ESI(+): calcd for  $\text{C}_{37}\text{H}_{38}\text{ClIrN}_3\text{O}_2$   $m/z$  = 784.2282  $[\text{M} + \text{H}]^+$ , found  $m/z$  = 784.2267.

**Preparation of L3.** In a 100 mL round-bottom flask, 2-picolinic acid (0.270 g, 2.2 mmol, 1.0 equiv) was dissolved in ~20 mL of anhydrous dichloromethane and cooled in an ice bath for ~15 min. Triethylamine (0.92 mL, 6.6 mmol, 3.0 equiv) was added to the reaction mixture and stirred for 15 min. The resulting solution was then treated with ethyl chloroformate (0.27 mL, 2.86 mmol, 1.3 equiv) and stirred in an ice bath for another 30 min before combining with **16** (0.490 g, 1.32 mmol, 0.6 equiv). The reaction was stirred in an ice bath for 1 h, warmed up to 25 °C, and stirred for another 24 h. Once the reaction was complete, water was added and the organic phase was separated, dried over sodium sulfate, filtered to remove the drying agent, and evaporated to dryness. The crude product was purified by silica gel column chromatography (20% ethyl acetate in hexane) to obtain a colorless oil (446 mg, 71% yield).  $^1\text{H}$  NMR ( $\text{CDCl}_3$ , 500 MHz):  $\delta$  8.53 (dd,  $J$  = 5.0, 1.7 Hz, 1H), 8.28 (d,  $J$  = 9.2 Hz, 1H), 8.23–8.08 (m, 5H), 8.07–7.95 (m, 4H), 7.89–7.78 (m, 2H), 7.43–7.35 (m, 1H), 3.46 (q,  $J$  = 6.9 Hz, 2H), 3.39–3.27 (m, 2H), 1.92–1.76 (m, 2H), 1.63 (t,  $J$  = 7.3 Hz, 2H), 1.51–1.44 (m, 2H), and 1.43–1.22 (m, 12H) ppm.  $^{13}\text{C}$  NMR (126 MHz,  $\text{CDCl}_3$ ):  $\delta$  164.32, 150.20, 148.10, 137.49, 137.44, 131.56, 131.06, 129.78, 128.71, 127.66, 127.38, 127.19, 126.58, 126.13, 125.86, 125.19, 124.89, 124.87, 124.72, 123.67, 122.30, 39.59, 33.75, 32.09, 29.94, 29.78, 29.71, 29.70, 29.64, 29.44, and 27.13 ppm. HRMS-ESI(+): calcd for  $\text{C}_{33}\text{H}_{36}\text{N}_2\text{O}_2\text{Na}$   $m/z$  = 499.2707  $[\text{M} + \text{Na}]^+$ , found  $m/z$  = 499.2725.

**Preparation of Ir3.** In a 50 mL Schlenk flask, 15 mL of dichloromethane was purged with nitrogen for about 10 min.  $[\text{Cp}^*\text{IrCl}_2]_2$  (208 mg, 0.260 mmol, 0.5 equiv) and ligand **L3** (298 mg, 0.625 mmol, 1.2 equiv) were added and stirred for 5 min at 25 °C. The reaction mixture was then treated with  $\text{Et}_3\text{N}$  (80  $\mu\text{L}$ , 0.18 mmol, 1.1 equiv) and stirred at room temperature for another 24 h. Once the reaction was complete, the reaction mixture was washed with water (3  $\times$  20 mL). The organic phase was separated, dried over sodium sulfate, filtered to remove the drying agent, and then evaporated to dryness. The crude product was purified by silica gel column chromatography (10% methanol in dichloromethane) to obtain a yellow solid (357 mg, 82% yield).  $^1\text{H}$  NMR ( $\text{CDCl}_3$ , 500 MHz):  $\delta$  8.49 (d,  $J$  = 5.5 Hz, 1H), 8.29 (d,  $J$  = 9.3 Hz, 1H), 8.17–8.08 (m, 4H), 8.08–7.95 (m, 4H), 7.90–7.82 (m, 2H), 7.38 (ddd,  $J$  = 7.3, 5.6, 1.6 Hz, 1H), 4.55 (ddd,  $J$  = 12.1, 9.9, 6.6 Hz, 1H), 3.33 (t,  $J$  = 7.9 Hz, 2H), 3.05 (ddd,  $J$  = 12.1, 10.0, 4.9 Hz, 1H), 1.88–1.80 (m, 2H), 1.73–1.67 (s, 4H), 1.61 (s, 15H), 1.50–1.43 (m, 2H), and 1.39–1.26 (m, 10H) ppm.  $^{13}\text{C}$  NMR (126 MHz,  $\text{CDCl}_3$ ):  $\delta$  169.92, 156.09, 148.90, 138.44, 137.66, 131.55, 131.08, 129.73, 128.71, 127.69, 127.45, 127.19, 126.70, 126.51, 126.05, 125.83, 125.16, 124.93, 124.80, 124.71, 123.76, 86.34, 50.49, 33.78, 32.14, 30.00, 29.86, 29.78, 29.76, 29.74, 29.72, 29.32, 27.87, and 8.90 ppm. IR ( $\bar{\nu}$ ): 2922, 2850,

1619, 1592, 1563, 1461, 1377, 1288, 1028, 845, 760, 720, 683, 617, and 506  $\text{cm}^{-1}$ . HRMS-ESI(+): calcd for  $\text{C}_{43}\text{H}_{51}\text{ClIrN}_2\text{O}$   $m/z$  = 839.3312  $[\text{M} + \text{H}]^+$ , found  $m/z$  = 839.3319. UV-vis in  $\text{H}_2\text{O}$  ( $\lambda_{\text{max}}$ ): 330 nm (29,076  $\text{M}^{-1} \text{cm}^{-1}$ ), and 350 nm (34,100  $\text{M}^{-1} \text{cm}^{-1}$ ). Emission in  $\text{H}_2\text{O}$  ( $\lambda_{\text{em}}$ ): 395 nm ( $\lambda_{\text{ex}}$  = 350 nm).

**Cell Culture.** Human neuroblastoma (SH-SY5Y) cells were purchased from the American Type Culture Collection (ATCC, Manassas, VA, USA). The cells were cultured in DMEM/F12 (1:1) supplemented with 10% heat-inactivated fetal bovine serum (FBS), 1% penicillin–streptomycin, and 2 mM GlutaMAX in 100  $\text{cm}^2$  tissue culture flasks. The culture was maintained under a humidified atmosphere of 5%  $\text{CO}_2$  at 37  $^\circ\text{C}$ . When  $\sim 80\%$  confluence was reached, cells were trypsinized (0.05% trypsin–EDTA) for subculture, and the media was replaced in every 3 day intervals. The cells were treated with 1.0 mM  $\text{MPP}^+$  iodide to develop a PD cell model.

**ICP–MS Analysis.** Cells were grown in 100 mm tissue culture plates at 37  $^\circ\text{C}$  under a 5%  $\text{CO}_2$  atmosphere. When  $\sim 70\%$  confluence was reached, the DMEM solution was removed by aspiration and replaced with a new DMEM solution containing the desired amount of Ir complex. At the end of the treatment period, the cells were washed twice with phosphate-buffered saline (PBS), detached by treatment with trypsin, and 10  $\mu\text{L}$  of the cell suspension was taken for cell counting. The trypsinized samples were then centrifuged and the supernatant was discarded. The cell pellet was washed with fresh DMEM and PBS through vortexing, centrifuging, and removing the supernatant. The cell pellets were digested using 0.2 mL of 65–70% metal-free distilled  $\text{HNO}_3$  at room temperature overnight. To each sample, 5.8 mL of HPLC-grade water was added to obtain a 2%  $\text{HNO}_3$  solution. The resulting cloudy solutions were centrifuged to obtain clear samples for ICP–MS analysis. A standard iridium solution (10  $\mu\text{g}/\text{mL}$ ) was diluted in 2%  $\text{HNO}_3$  solution to make a series of concentrations from 0 to 20 ppb. The iridium content of each sample was measured to establish a calibration curve. By using this calibration curve, the iridium concentrations in the lysate samples were determined. The final concentration of iridium was calculated using the following equation:  $[\text{Ir}]$  (ng/ $10^6$  cells) = (total Ir)/(total cells), and total Ir (ng) =  $[\text{Ir}]$  (in ppb)  $\times$  6.0 mL.

**Cytotoxicity Sulforhodamine B Assays.** Cells were seeded in a 96-well plate (Corning 3595) and incubated at 37  $^\circ\text{C}$  in a humidified atmosphere with 5%  $\text{CO}_2$  to allow them to adhere to the bottom of the wells ( $\sim 48$  h). Stock solutions of the test compounds were prepared in either DMSO or DMEM, then diluted in cell culture media (DMEM: F12 (1:1) supplemented with 10% fetal bovine serum (FBS)), 1% penicillin–streptomycin 100 $\times$  solution, and 2 mM GlutaMax to make the desired concentrations. The cell culture medium was replaced with fresh cell culture media containing the test compounds at different concentrations. The cells were then incubated for a desired amount of time. The solutions were removed by aspiration, and the cells were washed with fresh DMEM before 100  $\mu\text{L}$  of fresh cell culture medium (with no FBS) was added to each well, followed by 50  $\mu\text{L}$  of a fixative reagent (Cytoscan SRB Cytotoxicity Assay, G-Biosciences, catalog # 786-213). The 96-well plate was kept at 4  $^\circ\text{C}$  for 1 h and then the cells were washed 3 times with distilled water before drying for 2–3 h at 37  $^\circ\text{C}$ . A 100  $\mu\text{L}$  solution containing sulforhodamine B (SRB) was then added to each well and the 96-well plate was kept in the dark at RT for 30 min. The cells were then rinsed 4 times with a 1 $\times$  dye wash solution before drying for 2–3 h at 37  $^\circ\text{C}$ . A 200  $\mu\text{L}$  of SRB solubilization buffer was added to each well and mixed by pipetting the mixture up and down to dissolve the dye completely. The absorbance of the 96-well plate was then measured at 510 and 565 nm on a Tecan Infinite M200 Pro microplate reader. The cell viability was considered proportional to the absorbance measured. The average absorbance value of wells containing only solubilization buffer (background) was subtracted from that of wells containing treated and untreated cells. The percent cell viability was calculated using the following equation:  $(A_{\text{conc}}/A_{\text{control}}) \times 100\%$ , where  $A_{\text{conc}}$  is the absorbance of wells containing cells treated with specific concentrations of the test compound and  $A_{\text{control}}$  is the absorbance of wells containing untreated cells. The  $\text{IC}_{50}$

values were determined by fitting the data to a sigmoidal curve to obtain the concentrations at 50% cell viability.

**Detoxification Studies.** Cells were seeded in a 96-well plate (Corning 3595) and incubated at 37  $^\circ\text{C}$  with 5%  $\text{CO}_2$  for  $\sim 48$  h. The cell culture medium was removed by aspiration, and fresh medium containing the iridium complex or small organic compound was added. At the end of the treatment period, the solution was removed, and cells were washed twice with fresh medium. A solution containing the toxic aldehyde or  $\text{MPP}^+$  iodide in cell culture medium was then added, and the cells were incubated at 37  $^\circ\text{C}$  with 5%  $\text{CO}_2$  for the desired time. The cell viability was then measured using an SRB assay as described above. The detoxification efficiency of the iridium complexes or organic compounds was determined based on the number of cells alive relative to that of the control. The fold-change in cell viability was calculated as a ratio of the percentage of viable cells in treated wells divided by the percentage of viable cells in negative control wells (i.e., groups containing only toxic aldehyde or  $\text{MPP}^+$  iodide). The number of cells in the negative control wells with no treatment was considered as 100% cell viability.

**Reactive Oxygen Species Assays.** Cells were seeded in a clear bottom, black 96-well plate (Corning 3603) and incubated in a 5%  $\text{CO}_2$  humidified incubator for  $\sim 48$  h. The cells were then incubated with the iridium complex or organic compound for 3 h. Next, the medium was removed, and the cells were washed with fresh DMEM. The cell culture medium containing  $\text{MPP}^+$  iodide (1.0 mM) and  $\text{HCOONa}$  (1.0 mM) was added, and the cells were incubated at 37  $^\circ\text{C}$  with 5%  $\text{CO}_2$  for 24 h. At the end of the treatment period, the medium was removed, and the cells were washed with DMEM. Additional PBS (with 10% FBS) containing 2,7-dichlorofluorescein diacetate (DCFDA, Sigma S10 Aldrich, 10  $\mu\text{M}$ ) was then added, and the cells were incubated for 45 min at 37  $^\circ\text{C}$  in the dark. The ROS in each well was determined by exciting the sample at 485 nm and measuring the fluorescence intensity at 535 nm using a Tecan Infinite M200 Pro microplate reader. Cells treated with a 20  $\mu\text{M}$  *tert*-butyl hydrogen peroxide (TBHP) solution were used as a positive control for ROS. The fluorescence unit (FU) was determined by dividing the integrated fluorescence intensity obtained from each well by the number of viable cells in that well. The relative fluorescence unit (RFU) was calculated by dividing the fluorescence unit in each treated well by the fluorescence unit in the negative control well (no treatment). The fluorescence intensity is proportional to the intracellular concentration of ROS.

**Aldehyde Quantification Assays.** SH-SY5Y cells were cultured in tissue culture plates (Corning 430167) at 37  $^\circ\text{C}$  under a 5%  $\text{CO}_2$  atm for at least 2 d to maximize cell adherence. When  $\sim 70\%$  confluence was achieved, the medium was replaced with a fresh cell culture medium containing iridium complexes or organic compounds. The cells were then incubated at 37  $^\circ\text{C}$  under a 5%  $\text{CO}_2$  atm for 3 h, washed twice with DMEM, and incubated with  $\text{MPP}^+$  iodide (1.0 mM) and  $\text{HCOONa}$  (1.0 mM) for another 24 h. At the end of the treatment period, the medium was removed, and the cells were washed twice with fresh DMEM, detached by treating with trypsin, and 10  $\mu\text{L}$  of the cell suspension was taken for cell counting. The trypsinized cells were then centrifuged and the supernatant was removed. The cell pellets were washed with fresh DMEM and PBS (vortexed, centrifuged, and then the supernatant was removed). The washed cell pellets were mixed with 0.2 mL of 20 mM Tris–HCl (pH 7.4) and  $\sim 75$  mg of zirconium oxide beads (0.5 mm) and lysed at 4  $^\circ\text{C}$  using a Next Advance bullet blender tissue homogenizer BBX24B (speed 8, time 3). These samples were then centrifuged for 10 min at 2000g and 4  $^\circ\text{C}$  to obtain clear supernatants. In a clear bottom black 96-well plate (Corning 3603), 50  $\mu\text{L}$  of the cell lysate (or blank control, or aldehyde standard) was added into each well, followed by the addition of 50  $\mu\text{L}$  of aldehyde blue indicator assay solution (Abcam's fluorometric aldehyde quantification assay kit, product #ab138882). The plate was then protected from light and incubated at 25  $^\circ\text{C}$  for 30 min. Next, 25  $\mu\text{L}$  of buffer was added into each well and gently mixed by pipetting. The fluorescence intensity in each well was measured with excitation at 365 nm and emission at 435 nm. A set of aldehyde standards (0–1000  $\mu\text{M}$ , triplicates) was used to make

the calibration curve. The total aldehyde concentration was determined by dividing the integrated fluorescence intensity obtained from each well by the number of viable cells in each well. The fluorescence intensity is proportional to the intracellular concentration of aldehydes.

**JC-10 Mitochondrial Membrane Potential Assay.** Mitochondrial membrane potential was assessed using JC-10 assay (G-Biosciences, Cat. # 786-1541). SH-SY5Y cells were seeded in a clear bottom, black 96-well plate (Corning 3603) and incubated in a 5% CO<sub>2</sub> humidified incubator for approximately 48 h. The solution was aspirated and fresh cell culture medium containing either iridium complexes or organic compounds was added. The cells were then incubated at 37 °C under a 5% CO<sub>2</sub> atm for 3 h, washed twice with DMEM, and subsequently incubated with the MPP<sup>+</sup> iodide (1.0 mM) and HCOONa (1.0 mM) for an additional 24 h. Next, the cell culture medium was replaced with 100 μL of the working JC-10 dye solution, and the plate was incubated in an incubator for 40 min. The cells were then washed with 1× MMP-assay buffer solution. Finally, 100 μL of MMP-assay buffer was added to each well, and the plate was read using a microplate reader. The red fluorescence was measured at 595 nm emission with 535 nm excitation, while the green fluorescence was measured at 530 nm emission with 485 nm excitation. The data were expressed as the red/green fluorescence intensity ratios.

**NAD<sup>+</sup>/NADH Ratio Assay.** Experiments to determine intracellular NAD<sup>+</sup>/NADH ratio were performed using the NAD<sup>+</sup>/NADH ratio assay kit from AAT (Cat. #15273) following the manufacturer's protocols. Briefly, SH-SY5Y cells were cultured in 100 mm tissue culture plates at 37 °C under a 5% CO<sub>2</sub> atm for at least 2 d to maximize cell adherence. When ~70% confluence was achieved, the medium was replaced with fresh cell culture medium containing iridium complexes or organic compounds. The cells were then incubated at 37 °C under a 5% CO<sub>2</sub> atm for 3 h, washed twice with DMEM, and then incubated with the MPP<sup>+</sup> iodide (1.0 mM) and HCOONa (1.0 mM) for 24 h. At the end of the treatment period, the medium was removed, and the cells were washed twice with fresh DMEM. The cells were then detached by trypsin treatment, and 10 μL of the cell suspension was taken for cell counting. The trypsinized cells were then centrifuged, and the supernatant was discarded. The cell pellets were washed with fresh DMEM and PBS. The cells were lysed by treating with 200 μL of lysis buffer, and the resulting lysates were used to measure the NAD<sup>+</sup> and NADH concentrations. Based on the assay kit instructions, the concentration of NAD<sup>+</sup> and total [NAD<sup>+</sup> and NADH] were determined. The NAD<sup>+</sup> ratio was calculated as the following equation: NAD<sup>+</sup> ratio (%) = ([NAD<sup>+</sup>]/[total NAD<sup>+</sup> and NADH]) × 100%.

**Aldehyde Detoxification Studies.** Cells were seeded in a 96-well plate (Corning 3595) and incubated at 37 °C with 5% CO<sub>2</sub> for ~48 h. The cell culture medium was removed by aspiration, and fresh medium containing either the iridium complex or small organic compound was added. At the end of the treatment period, the solution was removed, and cells were washed twice with fresh medium. A solution containing the toxic aldehyde in cell culture medium was then added, and the cells were incubated at 37 °C with 5% CO<sub>2</sub> for the desired time. The cell viability was then measured using an SRB assay as described above. The detoxification efficiency of the iridium complexes or organic compounds was determined based on the number of cells alive relative to that of the control. The fold of cell viability was calculated as a ratio of the percentage of viable cells in treated wells divided by the percentage of viable cells in negative control wells (i.e., groups containing only toxic aldehyde). The number of cells in positive control wells with nontreatment conditions was considered as 100% cell viability.

**Detoxification Studies of MPP<sup>+</sup>-Treated Cells.** Cells were seeded in a 96-well plate (Corning 3595) and incubated at 37 °C with 5% CO<sub>2</sub> for approximately 48 h. After incubation, the cell culture medium was aspirated, and fresh medium containing either the iridium complex or small organic compound was added. After 3 h of incubation, the solution was removed, and cells were washed twice with PBS. A solution containing MPP<sup>+</sup> iodide (1.0 mM) and HCOONa (1.0 mM) in the cell culture medium was added, and the

cells were incubated at 37 °C with 5% CO<sub>2</sub> for 24 h. The cell viability was then measured using an SRB assay as described above. The detoxification efficiency of the iridium complexes or organic compounds was determined based on the number of cells alive relative to that of the control. The fold change in cell viability was calculated as a ratio of the percentage of viable cells in treated wells divided by the percentage of viable cells in negative control wells (i.e., groups containing only toxic aldehyde or MPP<sup>+</sup> iodide). The number of cells in positive control wells with nontreatment conditions was considered as 100% cell viability.

**Time-Dependent Detoxification Studies of MPP<sup>+</sup>-Treated Cells.** Cells were seeded in the 96-well plate (Corning 3595) and incubated at 37 °C with 5% CO<sub>2</sub> for ~48 h. The cell culture medium was replaced with fresh medium containing the iridium complex (5 μM) or small organic compounds (500 μM of Car, 50 μM of Rep, 500 μM of Asc, and 500 μM of L-dopa). After 3 h of treatment, the solution was removed, and cells were washed twice with PBS. A solution containing MPP<sup>+</sup> iodide (1.0 mM) and HCOONa (1.0 mM) in cell culture medium was added, and the cells were incubated at 37 °C with 5% CO<sub>2</sub> for 21 h. After incubation, the medium was removed, and the cells were washed twice with PBS. A fresh cell culture medium containing MPP<sup>+</sup> iodide (0.5 mM) and HCOONa (1.0 mM) was treated daily until day 5 (a total of 4 times on days 1, 2, 3, and 4). The iridium complex (5 μM) treatment procedure was repeated every other day (days 2 and 4). At the end of each treatment period, the medium was removed, and cells were washed twice with PBS. The cell viability was measured on days 1, 2, 4, and 6 using an SRB assay. The detoxification efficiency of the iridium complexes or organic compounds was assessed based on the number of cells alive relative to that of the control. The fold change in cell viability was calculated as a ratio of the percentage of viable cells in treated wells divided by the percentage of viable cells in negative control wells (i.e., groups containing only MPP<sup>+</sup> iodide). The number of cells in positive control wells with nontreatment conditions was considered to be 100% cell viability.

## ■ ASSOCIATED CONTENT

### Supporting Information

The Supporting Information is available free of charge at <https://pubs.acs.org/doi/10.1021/acs.jmedchem.4c02741>.

Detailed description of synthetic procedures, spectroscopic data, biological studies, and characterization data (PDF)

Molecular formula strings (CSV)

## ■ AUTHOR INFORMATION

### Corresponding Author

Loi H. Do – Department of Chemistry, University of Houston, Houston, Texas 77204, United States; [orcid.org/0000-0002-8859-141X](https://orcid.org/0000-0002-8859-141X); Email: [loido@uh.edu](mailto:loido@uh.edu)

### Authors

Rahul D. Jana – Department of Chemistry, University of Houston, Houston, Texas 77204, United States

Hieu D. Nguyen – Department of Chemistry, University of Houston, Houston, Texas 77204, United States; [orcid.org/0000-0002-0609-5106](https://orcid.org/0000-0002-0609-5106)

Guangjie Yan – Department of Chemistry, University of Houston, Houston, Texas 77204, United States

Tai-Yen Chen – Department of Chemistry, University of Houston, Houston, Texas 77204, United States; [orcid.org/0000-0002-2881-3068](https://orcid.org/0000-0002-2881-3068)

Complete contact information is available at:

<https://pubs.acs.org/10.1021/acs.jmedchem.4c02741>

## Author Contributions

R.D.J.: conceptualization, investigation, analysis, writing; H.D.N.: investigation; G.Y.: investigation; T.-Y.C.: supervision, funding acquisition; L.H.D.: conceptualization, funding acquisition, supervision, writing.

## Notes

The authors declare no competing financial interest.

## ACKNOWLEDGMENTS

We are grateful to the National Institute of General Medicine Sciences of the National Institutes of Health for funding this work (R01GM129276 to L.H.D. and R35GM133505 to T.-Y.C.).

## ABBREVIATIONS

ANOVA, analysis of variance; Asc, ascorbate; BBB, blood–brain barrier; C–I, Complex I of the mitochondria; Car, carnosine; CD, carbidopa; CoQ10, coenzyme Q10; Cp<sup>\*</sup>, pentamethylcyclopentadienyl anion; detox, detoxification; DCFDA, 2,7-dichlorofluorescein diacetate; DMEM, Dulbecco's Modified Eagle Medium; DMSO, dimethyl sulfoxide; DOPAL, 2,3-dihydroxyphenylacetaldehyde; L-Dopa, levodopa; FBS, fetal bovine serum; FU, fluorescence unit; 4-HNE, 4-hydroxynon-2-enal; HPLC, high performance liquid chromatography; IC<sub>50</sub>, 50% inhibition concentration; ICP-MS, inductively-coupled plasma mass spectrometry; IR, infrared; MMP, mitochondria membrane potential; MPP<sup>+</sup>, 1-methyl-4-phenylpyridinium; NAD<sup>+</sup>, oxidized nicotinamide adenine dinucleotide; NADH, reduced nicotinamide adenine dinucleotide; NMR, nuclear magnetic resonance; PAMPA, Parallel Artificial Membrane Permeability Assay; PBS, phosphate-buffered saline; PCC, Pearson correlation coefficient; PD, Parkinson's Disease; Py, pyrene; RASP, reactive aldehyde species; Rep, Reproxalap; RFU, relative fluorescence unit; SD, standard deviation; SRB, sulforhodamine B; ROS, reactive oxygen species; TBHP, *tert*-butyl hydrogen peroxide; TON, turnover number; UV–vis, ultraviolet–visible.

## REFERENCES

- (1) de Lau, L. M. L.; Breteler, M. M. B. Epidemiology of Parkinson's disease. *Lancet Neurol.* **2006**, *5*, 525–535.
- (2) Bloem, B. R.; Okun, M. S.; Klein, C. Parkinson's disease. *Lancet* **2021**, *397*, 2284–2303.
- (3) Ye, H.; Robak, L. A.; Yu, M.; Cykowski, M.; Shulman, J. M. Genetics and Pathogenesis of Parkinson's Syndrome. *Annu. Rev. Pathol. Mech. Dis.* **2023**, *18*, 95–121.
- (4) Ben-Shlomo, Y.; Darweesh, S.; Llibre-Guerra, J.; Marras, C.; San Luciano, M.; Tanner, C. The epidemiology of Parkinson's disease. *Lancet* **2024**, *403*, 283–292.
- (5) Morris, H. R.; Spillantini, M. G.; Sue, C. M.; Williams-Gray, C. H. The pathogenesis of Parkinson's disease. *Lancet* **2024**, *403*, 293–304.
- (6) Borsche, M.; Pereira, S. L.; Klein, C.; Grünwald, A. Mitochondria and Parkinson's Disease: Clinical, Molecular, and Translational Aspects. *J. Parkinson Dis.* **2021**, *11*, 45–60.
- (7) Polymeropoulos, M. H.; Lavedan, C.; Leroy, E.; Ide, S. E.; Dehejia, A.; Dutra, A.; Pike, B.; Root, H.; Rubenstein, J.; Boyer, R.; Stenroos, E. S.; Chandrasekharappa, S.; Athanassiadou, A.; Papapetropoulos, T.; Johnson, W. G.; Lazzarini, A. M.; Duvoisin, R. C.; Di Iorio, G.; Golbe, L. I.; Nussbaum, R. L. Mutation in the  $\alpha$ -Synuclein Gene Identified in Families with Parkinson's Disease. *Science* **1997**, *276*, 2045–2047.
- (8) Spillantini, M. G.; Schmidt, M. L.; Lee, V. M.-Y.; Trojanowski, J. Q.; Jakes, R.; Goedert, M.  $\alpha$ -Synuclein in Lewy bodies. *Nature* **1997**, *388*, 839–840.

- (9) Fusco, G.; Chen, S. W.; Williamson, P. T. F.; Cascella, R.; Perni, M.; Jarvis, J. A.; Cecchi, C.; Vendruscolo, M.; Chiti, F.; Cremades, N.; Ying, L.; Dobson, C. M.; De Simone, A. Structural basis of membrane disruption and cellular toxicity by  $\alpha$ -synuclein oligomers. *Science* **2017**, *358*, 1440–1443.

- (10) Calabresi, P.; Mechelli, A.; Natale, G.; Volpicelli-Daley, L.; Di Lazzaro, G.; Ghiglieri, V. Alpha-synuclein in Parkinson's disease and other synucleinopathies: from overt neurodegeneration back to early synaptic dysfunction. *Cell Death Dis.* **2023**, *14*, 176.

- (11) Pirooznia, S. K.; Rosenthal, L. S.; Dawson, V. L.; Dawson, T. M. Parkinson Disease: Translating Insights from Molecular Mechanisms to Neuroprotection. *Pharmacol. Rev.* **2021**, *73*, 1204–1268.

- (12) Chopade, P.; Chopade, N.; Zhao, Z.; Mitragotri, S.; Liao, R.; Suja, V. C. Alzheimer's and Parkinson's disease therapies in the clinic. *Bioeng. Transl. Med.* **2023**, *8*, No. e10367.

- (13) Armstrong, M. J.; Okun, M. S. Diagnosis and treatment of Parkinson disease: a review. *Jama* **2020**, *323*, 548–560.

- (14) Lane, E. L. L-DOPA for Parkinson's disease—a bittersweet pill. *Eur. J. Neurosci.* **2019**, *49*, 384–398.

- (15) Fahn, S.; Oakes, D.; Shoulson, I.; Kieburtz, K.; Rudolph, A.; et al. Levodopa and the Progression of Parkinson's Disease. *N. Engl. J. Med.* **2004**, *351*, 2498–2508.

- (16) Olanow, C. W.; Agid, Y.; Mizuno, Y.; Albanese, A.; Bonucelli, U.; Damier, P.; De Yebenes, J.; Gershanik, O.; Guttman, M.; Grandas, F.; Hallett, M.; Hornykiewicz, O.; Jenner, P.; Katzenschlager, R.; Langston, W. J.; LeWitt, P.; Melamed, E.; Mena, M. A.; Michel, P. P.; Mytilineou, C.; Obeso, J. A.; Poewe, W.; Quinn, N.; Raisman-Vozari, R.; Rajput, A. H.; Rascol, O.; Sampaio, C.; Stocchi, F. Levodopa in the Treatment of Parkinson's Disease: Current Controversies. *Mov. Disord.* **2004**, *19*, 997–1005.

- (17) Henchcliffe, C.; Beal, M. F. Mitochondrial biology and oxidative stress in Parkinson disease pathogenesis. *Nat. Clin. Pract. Neurol.* **2008**, *4*, 600–609.

- (18) Abou-Sleiman, P. M.; Muqit, M. M. K.; Wood, N. W. Expanding insights of mitochondrial dysfunction in Parkinson's disease. *Nat. Rev. Neurosci.* **2006**, *7*, 207–219.

- (19) Schapira, A. H. V.; Cooper, J. M.; Dexter, D.; Jenner, P.; Clark, J. B.; Marsden, C. D. Mitochondrial Complex I Deficiency in Parkinson's Disease. *Lancet* **1989**, *333*, 1269.

- (20) González-Rodríguez, P.; Zampese, E.; Stout, K. A.; Guzman, J. N.; Ilijic, E.; Yang, B.; Tkatch, T.; Stavarache, M. A.; Wokosin, D. L.; Gao, L.; Kaplitt, M. G.; López-Barneo, J.; Schumacker, P. T.; Surmeier, D. J. Disruption of mitochondrial complex I induces progressive parkinsonism. *Nature* **2021**, *599*, 650–656.

- (21) Raha, S.; Robinson, B. H. Mitochondria, oxygen free radicals, and apoptosis. *Am. J. Med. Genet.* **2001**, *106*, 62–70.

- (22) Angelova, P. R.; Abramov, A. Y. Role of mitochondrial ROS in the brain: from physiology to neurodegeneration. *FEBS Lett.* **2018**, *592*, 692–702.

- (23) Zielonka, J.; Joseph, J.; Sikora, A.; Hardy, M.; Ouari, O.; Vasquez-Vivar, J.; Cheng, G.; Lopez, M.; Kalyanaraman, B. Mitochondria-Targeted Triphenylphosphonium-Based Compounds: Syntheses, Mechanisms of Action, and Therapeutic and Diagnostic Applications. *Chem. Rev.* **2017**, *117*, 10043–10120.

- (24) Xu, J.; Du, W.; Zhao, Y.; Lim, K.; Lu, L.; Zhang, C.; Li, L. Mitochondria targeting drugs for neurodegenerative diseases—Design, mechanism and application. *Acta Pharmacol. Sin.* **2022**, *12*, 2778–2789.

- (25) Jin, H.; Kanthasamy, A.; Ghosh, A.; Anantharam, V.; Kalyanaraman, B.; Kanthasamy, A. G. Mitochondria-targeted antioxidants for treatment of Parkinson's disease: Preclinical and clinical outcomes. *BBA, Mol. Basis Dis.* **2014**, *1842*, 1282–1294.

- (26) Beal, M. F.; Oakes, D.; Shoulson, I.; Henchcliffe, C.; Galpern, W. R.; Haas, R.; Juncos, J. L.; Nutt, J. G.; Voss, T. S.; Ravina, B.; et al. A Randomized Clinical Trial of High-Dosage Coenzyme Q10 in Early Parkinson Disease: No Evidence of Benefit. *JAMA Neurol* **2014**, *71*, 543–552.

- (27) Yoritaka, A.; Kawajiri, S.; Yamamoto, Y.; Nakahara, T.; Ando, M.; Hashimoto, K.; Nagase, M.; Saito, Y.; Hattori, N. Randomized, double-blind, placebo-controlled pilot trial of reduced coenzyme Q<sub>10</sub> for Parkinson's disease. *Parkinsonism Relat. Disord.* **2015**, *21*, 911–916.
- (28) Capriglia, F.; Burgess, T.; Bandmann, O.; Mortiboys, H. Clinical Trial Highlights: Modulators of Mitochondrial Function. *J. Parkinson's Dis.* **2023**, *13*, 851–864.
- (29) Zhu, Z.-G.; Sun, M.-X.; Zhang, W.-L.; Wang, W.-W.; Jin, Y.-M.; Xie, C.-L. The efficacy and safety of coenzyme Q<sub>10</sub> in Parkinson's disease: a meta-analysis of randomized controlled trials. *Neurol. Sci.* **2017**, *38*, 215–224.
- (30) Snow, B. J.; Rolfe, F. L.; Lockhart, M. M.; Frampton, C. M.; O'Sullivan, J. D.; Fung, V.; Smith, R. A. J.; Murphy, M. P.; Taylor, K. M. A double-blind, placebo-controlled study to assess the mitochondria-targeted antioxidant MitoQ as a disease-modifying therapy in Parkinson's disease. *Mov. Disord.* **2010**, *25*, 1670–1674.
- (31) Ellis, E. M. Reactive carbonyls and oxidative stress: Potential for therapeutic intervention. *Pharmacol. Ther.* **2007**, *115*, 13–24.
- (32) Di Domenico, F.; Tramutola, A.; Butterfield, D. A. Role of 4-hydroxy-2-nonenal (HNE) in the pathogenesis of Alzheimer disease and other selected age-related neurodegenerative disorders. *Free Radic. Bio. Med.* **2017**, *111*, 253–261.
- (33) Peña-Bautista, C.; Vento, M.; Baquero, M.; Cháfer-Pericás, C. Lipid peroxidation in neurodegeneration. *Clin. Chim. Acta* **2019**, *497*, 178–188.
- (34) Rodríguez-Zavala, J. S.; Calleja, L. F.; Moreno-Sánchez, R.; Yoval-Sánchez, B. Role of Aldehyde Dehydrogenases in Physiopathological Processes. *Chem. Res. Toxicol.* **2019**, *32*, 405–420.
- (35) Andersen, C.; Grnemoose, A. L.; Pedersen, J. N.; Nowak, J. S.; Christiansen, G.; Nielsen, J.; Mulder, F. A. A.; Otzen, D. E.; Jrgensen, T. J. D. Lipid Peroxidation Products HNE and ONE Promote and Stabilize Alpha-Synuclein Oligomers by Chemical Modifications. *Biochemistry* **2021**, *60*, 3644–3658.
- (36) Li, Y.; Zhao, T.; Li, J.; Xia, M.; Li, Y.; Wang, X.; Liu, C.; Zheng, T.; Chen, R.; Kan, D.; Xie, Y.; Song, J.; Feng, Y.; Yu, T.; Sun, P. Oxidative Stress and 4-hydroxy-2-nonenal (4-HNE): Implications in the Pathogenesis and Treatment of Aging-related Diseases. *J. Immunol. Res.* **2022**, *2022*, 2233906.
- (37) Masato, A.; Plotegher, N.; Terrin, F.; Sandre, M.; Faustini, G.; Thor, A.; Adams, S.; Berti, G.; Cogo, S.; De Lazzari, F.; Fontana, C. M.; Martinez, P. A.; Strong, R.; Bandopadhyay, R.; Bisaglia, M.; Bellucci, A.; Greggio, E.; Dalla Valle, L.; Boassa, D.; Bubacco, L. DOPAL initiates  $\alpha$ -Synuclein-dependent impaired proteostasis and degeneration of neuronal projections in Parkinson's disease. *npj Parkinson's Dis.* **2023**, *9*, 42.
- (38) Wood, P. L.; Khan, M. A.; Kulow, S. R.; Mahmood, S. A.; Moskal, J. R. Neurotoxicity of reactive aldehydes: The concept of "aldehyde load" as demonstrated by neuroprotection with hydroxylamines. *Brain Res.* **2006**, *1095*, 190–199.
- (39) Li, S. W.; Lin, T.-S.; Minter, S.; Burke, W. J. 3, 4-Dihydroxyphenylacetaldehyde and hydrogen peroxide generate a hydroxyl radical: possible role in Parkinson's disease pathogenesis. *Mol. Brain Res.* **2001**, *93*, 1–7.
- (40) Burke, W. J. 3, 4-Dihydroxyphenylacetaldehyde: A Potential Target for Neuroprotective Therapy in Parkinson's Disease. *Curr. Drug Targets CNS Neurol. Disord.* **2003**, *2*, 143–148.
- (41) Plotegher, N.; Berti, G.; Ferrari, E.; Tessari, I.; Zanetti, M.; Lunelli, L.; Greggio, E.; Bisaglia, M.; Veronesi, M.; Girotto, S.; Dalla Serra, M.; Perego, C.; Casella, L.; Bubacco, L. DOPAL derived alpha-synuclein oligomers impair synaptic vesicles physiological function. *Sci. Rep.* **2017**, *7*, 40699.
- (42) Näsström, T.; Wahlberg, T.; Karlsson, M.; Nikolajeff, F.; Lannfelt, L.; Ingelsson, M.; Bergström, J. The lipid peroxidation metabolite 4-oxo-2-nonenal cross-links  $\alpha$ -synuclein causing rapid formation of stable oligomers. *Biochem. Biophys. Res. Commun.* **2009**, *378*, 872–876.
- (43) Plotegher, N.; Bubacco, L. Lysines Achilles' heel in alpha-synuclein conversion to a deadly neuronal endotoxin. *Ageing Res. Rev.* **2016**, *26*, 62–71.
- (44) Laskar, A. A.; Younus, H. Aldehyde toxicity and metabolism: the role of aldehyde dehydrogenases in detoxification, drug resistance and carcinogenesis. *Drug. Metab. Rev.* **2019**, *51*, 42–64.
- (45) Masato, A.; Sandre, M.; Antonini, A.; Bubacco, L. Patients Stratification Strategies to Optimize the Effectiveness of Scavenging Biogenic Aldehydes: Towards a Neuroprotective Approach for Parkinson's Disease. *Curr. Neuropharmacol.* **2021**, *19*, 1618–1639.
- (46) Miranda, C. L.; Reed, R. L.; Kuiper, H. C.; Alber, S.; Stevens, J. F. Ascorbic Acid Promotes Detoxification and Elimination of 4-Hydroxy-2(E)-nonenal in Human Monocytic THP-1 Cells. *Chem. Res. Toxicol.* **2009**, *22*, 863–874.
- (47) Zhu, Q.; Zheng, Z.-P.; Cheng, K.-W.; Wu, J.-J.; Zhang, S.; Tang, Y. S.; Sze, K.-H.; Chen, J.; Chen, F.; Wang, M. Natural Polyphenols as Direct Trapping Agents of Lipid Peroxidation-Derived Acrolein and 4-Hydroxy-trans-2-nonenal. *Chem. Res. Toxicol.* **2009**, *22*, 1721–1727.
- (48) Böhme, A.; Thaens, D.; Schramm, F.; Paschke, A.; Schüürmann, G. Thiol Reactivity and Its Impact on the Ciliate Toxicity of  $\alpha,\beta$ -Unsaturated Aldehydes, Ketones, and Esters. *Chem. Res. Toxicol.* **2010**, *23*, 1905–1912.
- (49) Xie, Z.; Baba, S. P.; Sweeney, B. R.; Barski, O. A. Detoxification of Aldehydes by Histidine-Containing Dipeptides: From Chemistry to Clinical Implications. *Chem.-Biol. Interact.* **2013**, *202*, 288–297.
- (50) Mandell, K. J.; Clark, D.; Chu, D. S.; Foster, C. S.; Sheppard, J.; Brady, T. C. Randomized Phase 2 Trial of Reproxalap, a Novel Reactive Aldehyde Species Inhibitor, in Patients with Noninfectious Anterior Uveitis: Model for Corticosteroid Replacement. *J. Ocul. Pharmacol. Ther.* **2020**, *36*, 732–739.
- (51) Clark, D.; Cavanagh, B.; Shields, A. L.; Karpecki, P.; Sheppard, J.; Brady, T. C. Clinically Relevant Activity of the Novel RASP Inhibitor Reproxalap in Allergic Conjunctivitis: The Phase 3 ALLEVIATE Trial. *Am. J. Ophthalmol.* **2021**, *230*, 60–67.
- (52) Jana, R. D.; Ngo, A. H.; Bose, S.; Do, L. H. Organoiridium Complexes Enhance Cellular Defense Against Reactive Aldehydes Species. *Chem.—Eur. J.* **2023**, *29*, No. e202300842.
- (53) Bose, S.; Ngo, A. H.; Do, L. H. Intracellular Transfer Hydrogenation Mediated by Unprotected Organoiridium Catalysts. *J. Am. Chem. Soc.* **2017**, *139*, 8792–8795.
- (54) Ngo, A. H.; Ibañez, M.; Do, L. H. Catalytic hydrogenation of cytotoxic aldehydes using nicotinamide adenine dinucleotide (NADH) in cell growth media. *ACS Catal.* **2016**, *6*, 2637–2641.
- (55) Deza-Ponzio, R.; Herrera, M. L.; Bellini, M. J.; Virgolini, M. B.; Hereñú, C. B. Aldehyde dehydrogenase 2 in the spotlight: The link between mitochondria and neurodegeneration. *Neurotoxicology* **2018**, *68*, 19–24.
- (56) Almodares, Z.; Lucas, S. J.; Crossley, B. D.; Basri, A. M.; Pask, C. M.; Hebden, A. J.; Phillips, R. M.; McGowan, P. C. Rhodium, Iridium, and Ruthenium Half-Sandwich Picolinamide Complexes as Anticancer Agents. *Inorg. Chem.* **2014**, *53*, 727–736.
- (57) Hoye, A. T.; Davoren, J. E.; Wipf, P.; Fink, M. P.; Kagan, V. E. Targeting Mitochondria. *Acc. Chem. Res.* **2008**, *41*, 87–97.
- (58) Tomás-Gamasa, M.; Martínez-Calvo, M.; Couceiro, J. R.; Mascareñas, J. L. Transition metal catalysis in the mitochondria of living cells. *Nat. Commun.* **2016**, *7*, 12538.
- (59) Glushko, V.; Thaler, M. S. R.; Karp, C. D. Pyrene fluorescence fine structure as a polarity probe of hydrophobic regions: Behavior in model solvents. *Arch. Biochem. Biophys.* **1981**, *210*, 33–42.
- (60) Ngo, A. H.; Do, L. H. Structure–Activity Relationship Study of Half-Sandwich Metal Complexes in Aqueous Transfer Hydrogenation Catalysis. *Inorg. Chem. Front.* **2020**, *7*, 583–591.
- (61) Bradley, M. A.; Xiong-Fister, S.; Markesbery, W. R.; Lovell, M. A. Elevated 4-Hydroxyhexenal in Alzheimer's Disease (AD) Progression. *Neurobiol. Ageing* **2012**, *33*, 1034–1044.
- (62) Hodges, G.; Eadsforth, C.; Bossuyt, B.; Bouvy, A.; Enrici, M.-H.; Geurts, M.; Kotthoff, M.; Michie, E.; Miller, D.; Müller, J.; Oetter, G.; Roberts, J.; Schowanek, D.; Sun, P.; Venzmer, J. A comparison of

log  $K_{ow}$  (*n*-octanol–water partition coefficient) values for non-ionic, anionic, cationic and amphoteric surfactants determined using predictions and experimental methods. *Envir. Sci. Eur.* **2019**, *31*, 1.

(63) Agholme, L.; Lindström, T.; Kågedal, K.; Marcusson, J.; Hallbeck, M. An in vitro model for neuroscience: differentiation of SH-SY5Y cells into cells with morphological and biochemical characteristics of mature neurons. *J. Alzheimers Dis.* **2010**, *20*, 1069–1082.

(64) Xicoy, H.; Wieringa, B.; Martens, G. J. M. The SH-SY5Y cell line in Parkinson's disease research: a systematic review. *Mol. Neurodegener.* **2017**, *12*, 10.

(65) Lopez-Suarez, L.; Awabdh, S. A.; Coumoul, X.; Chauvet, C. The SH-SY5Y human neuroblastoma cell line, a relevant in vitro cell model for investigating neurotoxicology in human: Focus on organic pollutants. *Neurotoxicology* **2022**, *92*, 131–155.

(66) Anderson, E. J.; Katunga, L. A.; Willis, M. S. Mitochondria as a source and target of lipid peroxidation products in healthy and diseased heart. *Clin. Exp. Pharmacol. Physiol.* **2012**, *39*, 179–193.

(67) Langston, J. W.; Ballard, P.; Tetrud, J. W.; Irwin, I. Chronic Parkinsonism in Humans Due to a Product of Meperidine-Analog Synthesis. *Science* **1983**, *219*, 979–980.

(68) Bradbury, A. J.; Costall, B.; Domeney, A. M.; Jenner, P.; Kelly, M. E.; Marsden, C. D.; Naylor, R. J. 1-Methyl-4-phenylpyridine is neurotoxic to the nigrostriatal dopamine pathway. *Nature* **1986**, *319*, 56–57.

(69) Gerlach, M.; Riederer, P.; Przuntek, H.; Youdim, M. B. H. MPTP mechanisms of neurotoxicity and their implications for Parkinson's disease. *Eur. J. Pharmacol. Mol. Pharmacol.* **1991**, *208*, 273–286.

(70) Ramachandiran, S.; Hansen, J. M.; Jones, D. P.; Richardson, J. R.; Miller, G. W. Divergent Mechanisms of Paraquat, MPP<sup>+</sup>, and Rotenone Toxicity: Oxidation of Thioredoxin and Caspase-3 Activation. *Toxicol. Sci.* **2007**, *95*, 163–171.

(71) Tryphena, K. P.; Nikhil, U. S.; Pinjala, P.; Srivastava, S.; Singh, S. B.; Khatri, D. K. Mitochondrial Complex I as a Pathologic and Therapeutic Target for Parkinson's Disease. *ACS Chem. Neurosci.* **2023**, *14*, 1356–1368.

(72) Abarikwu, S. O.; Pant, A. B.; Farombi, E. O. 4-Hydroxynonenal Induces Mitochondrial-Mediated Apoptosis and Oxidative Stress in SH-SY5Y Human Neuronal Cells. *Basic Clin. Pharmacol. Toxicol.* **2012**, *110*, 441–448.

(73) King, M. S.; Sharpley, M. S.; Hirst, J. Reduction of Hydrophilic Ubiquinones by the Flavin in Mitochondrial NADH:Ubiquinone Oxidoreductase (Complex I) and Production of Reactive Oxygen Species. *Biochemistry* **2009**, *48*, 2053–2062.

(74) Jones, A. J. Y.; Blaza, J. N.; Bridges, H. R.; May, B.; Moore, A. L.; Hirst, J. A Self-Assembled Respiratory Chain that Catalyzes NADH Oxidation by Ubiquinone-10 Cycling between Complex I and the Alternative Oxidase. *Angew. Chem., Int. Ed.* **2016**, *55*, 728–731.

(75) Guan, L.; Yang, H.; Cai, Y.; Sun, L.; Di, P.; Li, W.; Liu, G.; Tang, Y. ADMET-score – a comprehensive scoring function for evaluation of chemical drug-likeness. *Med. Chem. Commun.* **2019**, *10*, 148–157.

(76) Law, V.; Knox, C.; Djoumbou, Y.; Jewison, T.; Guo, A. C.; Liu, Y.; Maciejewski, A.; Arndt, D.; Wilson, M.; Neveu, V.; Tang, A.; Gabriel, G.; Ly, C.; Adamjee, S.; Dame, Z. T.; Han, B.; Zhou, Y.; Wishart, D. S. DrugBank 4.0: shedding new light on drug metabolism. *Nucleic Acids Res.* **2014**, *42*, D1091–D1097.

(77) Bennion, B. J.; Be, N. A.; McNerney, M. W.; Lao, V.; Carlson, E. M.; Valdez, C. A.; Malfatti, M. A.; Enright, H. A.; Nguyen, T. H.; Lightstone, F. C.; Carpenter, T. S. Predicting a Drug's Membrane Permeability: A Computational Model Validated With in Vitro Permeability Assay Data. *J. Phys. Chem. B* **2017**, *121*, 5228–5237.

(78) Radan, M.; Djikic, T.; Obradovic, D.; Nikolic, K. Application of in vitro PAMPA technique and in silico computational methods for blood-brain barrier permeability prediction of novel CNS drug candidates. *Eur. J. Pharm. Sci.* **2022**, *168*, 106056.

(79) Sánchez-Martínez, J. D.; Valdés, A.; Gallego, R.; Suárez-Montenegro, Z. J.; Alarcón, M.; Ibañez, E.; Alvarez-Rivera, G.;

Cifuentes, A. Blood–Brain Barrier Permeability Study of Potential Neuroprotective Compounds Recovered From Plants and Agri-Food by-Products. *Front. Nutr.* **2022**, *9*, 924596.

(80) Gomes, L. M. F.; Bataglioli, J. C.; Storr, T. Metal complexes that bind to the amyloid- $\beta$  peptide of relevance to Alzheimer's disease. *Coord. Chem. Rev.* **2020**, *412*, 213255.

(81) Grcic, L.; Leech, G.; Kwan, K.; Storr, T. Targeting misfolding and aggregation of the amyloid- $\beta$  peptide and mutant p53 protein using multifunctional molecules. *Chem. Commun.* **2024**, *60*, 1372–1388.

(82) Navale, G. R.; Ahmed, I.; Lim, M. H.; Ghosh, K. Transition Metal Complexes as Therapeutics: A New Frontier in Combatting Neurodegenerative Disorders through Protein Aggregation Modulation. *Adv. Healthc. Mater.* **2024**, *13*, 2401991.

(83) Bataglioli, J. C.; Gomes, L. M. F.; Maunoir, C.; Smith, J. R.; Cole, H. D.; McCain, J.; Sainuddin, T.; Cameron, C. G.; McFarland, S. A.; Storr, T. Modification of amyloid-beta peptide aggregation via photoactivation of strained Ru(II) polypyridyl complexes. *Chem. Sci.* **2021**, *12*, 7510–7520.